DEVELOPMENT OF A NOVEL LOW-PRESSURE NANOFILTRATION MEMBRANE FOR Li^+/Mg^{2+} SEPARATION

A Thesis Submitted to the
Graduate School of Engineering and Sciences of
İzmir Institute of Technology
in Partial Fulfillment of the Requirements for the Degree of

MASTER OF SCIENCE

in Chemical Engineering

by
İsmail Tunahan ASLIYÜCE

December 2023
İZMİR

We approve the thesis of **İsmail Tunahan ASLIYÜCE.**

Examining Committee Members:

Prof. Dr. Sacide ALSOY ALTINKAYA
Department of Chemical Engineering, İzmir Institute of Technology

Prof. Dr. Nalan KABAY
Department of Chemical Engineering, Ege University

Assoc. Prof. Dr. Ayben TOP
Department of Chemical Engineering, İzmir Institute of Technology

12 December 2023

Prof. Dr. Sacide ALSOY ALTINKAYA
Supervisor, Department of Chemical Engineering,
İzmir Institute of Technology

Prof Dr. Aysun SOFUOĞLU
Head of the Department of
Chemical Engineering

Prof Dr. Mehtap EANES
Dean of the Graduate School of
Engineering and Science

ACKNOWLEDGMENT

ABSTRACT

DEVELOPMENT OF A NOVEL LOW-PRESSURE NANOFILTRATION MEMBRANE FOR Li^+/Mg^{2+} SEPARATION

Lithium-based batteries stand out as a crucial technology for energy storage. Between 2020 and 2022, lithium production surged from 77,000 to 100,000 tons. The majority of the world's lithium reserves are situated in water resources. Nevertheless, the direct extraction of lithium requires additional chemical processes due to the presence of other salts. Nanofiltration is recommended as an environmentally friendly and economical method for lithium purification. The main objective of this thesis is to develop a nanofiltration membrane for efficient Li^+ and Mg^{2+} separation. The support membrane was prepared through the phase inversion technique using polyamide-imide (PAI) in the casting solution and polyethyleneimine in the coagulation bath. In-situ dopamine polymerization under oxygen backflow formed an intermediate layer on the support surface for further modification. PDA-modified support was first coated with polyethyleneimine (PEI) functionalized alumina particles and then low molecular weight PEI (800Da). The final membrane design was optimized for Li^+ purity and Li^+ recovery. The produced nanofiltration membrane exhibited significant rejection rates, notably around ~90% % for Mg^{2+} and approximately ~ -21% for Li^+. Additionally, it demonstrated a pure water permeability of 9.7 L/m^2hbar. Each membrane layer underwent characterization through various techniques, including SEM, EDX, zeta potential analysis, AFM, and contact angle measurements. The membrane was subjected to stability tests under dynamic and static conditions. Li^+ and Mg^{+2} rejections, separation factor, and salt solution flux did not change after 30 days of storage in 2000 ppm salt solution and during 72 h dynamic filtration test.

ÖZET

Li^+/Mg^{+2} AYRIMI İÇİN ÖZGÜN BİR DÜŞÜK-BASINÇ NANOFİLTRASYON MEMBRANI GELİŞTİRİLMESİ

Lityum temelli bataryalar enerji depolama için kullanılan en önemli teknolojilerden biridir Lityum üretim miktarı 2020 yılından 2022 yılına kadar 77.000 tondan 100.000 tona çıkmıştır. Dünya genelinde lityum rezervlerinin büyük kısmı su kaynaklarında bulunmaktadır ancak diğer tuzların varlığı sebebiyle, bu kaynaklardan lityum üretmek için ek kimyasal süreçlerin kullanılması gerekmektedir. Nanofiltrasyon lityumu saflaştırmak için ekonomik ve çevre dostu bir yöntem olarak önerilmiştir. Bu tezin ana amacı Li^+ ve Mg^{+2} ayrımı için etkin bir nanofiltrasyon membranı geliştirmektir. Destek membranı poliamid-imid (PAI) kullanılarak faz değişim yöntemi ile hazırlanmıştır ve polietileniminli (PEI) koagülasyon banyosunda bekletilmiştir. Destek membranının modifikasyonu için yüzeyinde oksijen gaz akışı altında doğrudan dopamin polimerizasyonu ile bir ara katman oluşturulmuştur. PDA kaplı destek membranı önce PEI ile fonksiyonelleştirilmiş alümina parçacıklarıyla, ardından düşük molekül ağırlıklı PEI (800 Da) ile kaplanmıştır. Bu basamaklarla hazırlanmış olan membran, Li^+ saflığı ve Li^+ geri kazanımı göz önüne alınarak optimize edilmiştir. Üretilen nanofiltrasyon membranı Mg^{2+} iyonunun 90%'nının, Li^+ iyonunun ise -21%'nin geçişini engellemiştir. Ek olarak, optimum membranın saf su geçirgenliği 9.7 L/m^2saatbar'dır. Her bir membran katmanı, Taramalı Elektron Mikroskobu (SEM), Enerji Dağılımlı X-Ray Analizi (EDX), Zeta Potansiyeli, Atomik Kuvvet Mikroskobu (AFM) ve Temas Açı ölçümü ile karakterize edilmiştir. Membran, dinamik ve statik koşullar altında kararlılık testine tabii tutulmuştur. 30 günlük 2000 ppmlik tuz çözeltisinde bekletme ve 72 saatlik dinamik filtrasyon testlerinden sonra membranın Li^+ and Mg^{2+} iyonlarını alıkoyma oranları, ayırma faktörü ve tuz çözeltisi akısı gibi parametrelerinde bir değişim gözlenmemiştir.

TABLE OF CONTENT

LIST OF FIGURES

LIST OF TABLES

CHAPTER 1

INTRODUCTION

Lithium production has gained attention due to the development of energy storage solutions. Lithium-ion batteries, heavily reliant on lithium, are widely used in devices like smartphones, laptops, and electric vehicles. These batteries are needed for storing renewable energy generated from solar and wind power, helping us move towards a cleaner energy future. Additionally, lithium and its compounds find use in various industries, such as ceramics, glass, lubricants, and greases. From an economic perspective, lithium production plays a significant role[1]. According to the US Mineral Commodity Summaries of 2020 and 2022[2,3] annual lithium production ranged from 77,000 to 100,000 metric tons between 2019 and 2021. In 2016, 35% of the produced Li was used in battery systems, 32% in ceramics and glass industry, 9% in lubricating greases, and 24% in other industries[4]. However, by 2022, 74% of the produced Li used was directed towards battery systems, 14% to ceramics and glass industry, 3% to lubricating greases, and 9% to other industries[5]. In response to the growth in demand from developed economies, which was primarily driven by advancements in the production of portable lithium-ion batteries and battery packs, and to a lesser extent, the glass and ceramics industries, global lithium raw material production showed a rise.

Lithium can be produced from a variety of resources, including brine deposits, hard rock minerals, and geothermal brine[6]. Nearly 60% of Li resources are found in continental brines, and 25% in hard rocks. Depending on the lithium's source, the extraction process might require mining, pumping, or drilling to access the substance. However, Li production in aqueous sources is more practical and profitable than ore mining[4]. Countries with substantial lithium reserves, such as Australia, Chile, China, and Argentina, benefit from job creation, investment opportunities, and overall economic growth due to the development of their lithium industries[4–6]. Aqueous extraction methods, such as solar evaporation or direct extraction, are more energy efficient, resulting in cost savings and a reduced carbon footprint. Moreover, aqueous lithium production can extract other valuable minerals, promoting resource efficiency. While lithium-rich salt lakes like Salar de Atacama in Chile and Zabuye in China require minimal treatment, most other

salt lakes need pretreatment since Li^+ concentration in brine is low while co-ion concentrations are high. Simple solar evaporation process can only be used for pretreatment when the mass ratio of Mg^{2+}/Li^+ <6. In cases where the Mg^{2+}/Li^+ ratio is above 6, Li^+ ions form the complex crystalline structure, $MgCl_2.LiCl.7H_2O$ causing a decrease in Li^+ recovery rate[7]. The Mg^{2+}/Li^+ in most worldwide salt-lake brines is >8 [1], thus, effective technologies to increase Li^+ concentration in brine becomes the challenge in practical applications.

There are different methods for Li purification, including, adsorption using organic adsorbents or inorganic adsorbents, precipitation, solvent extraction, and electrochemical methods. In the industry, adsorption is the most commonly used method; however, it requires regeneration, operation is pH dependent and there is also disposal problem of used resins. Precipitation, on the other hand, cannot be used directly since Mg^{2+} salt concentration is too high for Li^+ precipitation in most sources. Also, it requires significant chemical usage, generates sludge, and has moderate efficiency. Electrochemical processes demand substantial energy that increases operational cost, and their probes need frequent replacement. Solvent extraction methods are not feasible for diluted target salts in industrial use. Thus, the current extraction processes consume considerable energy and water[1]. The conventional approach to separating lithium from brines relies on a dry environment, extensive sunlight, and considerable, environmentally harmful salt flats. The process's inherent slowness, and its demands for both land and freshwater, raise issues regarding its long-term sustainability. To achieve the desired manufacturing capacity for lithium-brine quickly and efficiently, a novel approach is required[8].The nanofiltration (NF) membrane demonstrates significant potential for Mg^{2+}/Li^+ separation from brine lakes as a result of combined effects of the Donnan exclusion, size exclusion, and dielectric exclusion. NF membranes allow Li^+ ions to pass through with water molecules while retaining larger metal ions. The efficient separation of Li^+ and Mg^{2+} using NF membranes facilitates the implementation of essential processes, resulting in reduced energy and material consumption, minimized salt flat requirements, and accelerated solar evaporation processes. Overall, NF plays a crucial role in efficient and sustainable lithium extraction, supporting the increasing demand for lithium-ion batteries in various industries.

The commercial NF membrane including NF270, Desal (DL), DK, etc., and NF90, have been tested for Li recovery [9]. The negative charge of commercial membranes limits their ability to separate Mg^{2+} and Li^+ due to similar hydrated ion radii of Mg^{2+}

(0.428 nm) and Li^+ (0.382 nm). To overcome this challenge, in recent years, researchers focused on developing positively charged NF membranes to benefit from Donnan exclusion. NF membranes were mostly prepared in thin film composite structure and the selective layer was made up of polyamide through interfacial polymerization (IP). During IP process, either the monomer type was changed, or additives were added to change the pore size and surface charge of the membrane[5]. In addition, the nanomaterials, such as, zeolites, metal organic frameworks (MOFs), covalent organic frameworks (COFs), carbon nanotubes (CNTs), graphene oxide (GO) and other two-dimensional (2D) materials were added to the selective layer to improve water permeability of the membranes[5]. Another strategy applied to develop positively charged NF membranes is to introduce specific functional groups by surface modification or grafting[5]. Other recent novel strategies include substrate modification[5] and layer by layer deposition of polyelectrolytes on the support membrane [5].

All the previous studies, focused on developing NF membranes for Li^+/Mg^{2+} separation, evaluated the membrane performance based on Li^+/Mg^{2+} selectivity and water permeability. However, recently, the analysis performed by Wang et al.[10] showed that these parameters are not sufficient performance criteria for evaluating the NF membrane. Instead, their study suggested that Li^+ purity and recovery should be taken into account as the first performance criteria.

Given that the primary objective of Li^+/Mg^{2+} separation is the production of lithium products, the critical factor is the recovery rate of lithium, which takes precedence over permeability. The membrane separation process must enhance the profitability of the production operation. The final output of the membrane separation becomes the feed stream for the lithium production process. While existing literature emphasizes the desire for high permeability and low magnesium salt concentration in the permeate stream, the key to profitability improvement lies in reducing magnesium concentration and water flux while simultaneously increasing lithium permeability.

This study aimed to develop a NF membrane based on layer-by-layer modification of the polyamide-imide (PAI) based support. To limit the number of layers, the pore size of the support was reduced by adding polyethylene imine (PEI) into the coagulation bath. An intermediate polydopamine layer was formed on the support through dopamine polymerization under oxygen backflow. Next, PEI-functionalized alumina particles were attached on the dopamine surface, and finally, to fill the uncovered polydopamine surface, low molecular weight PEI was impregnated. Different than the existing framework for

evaluating the performance of NF membranes, in this thesis, the final membrane structure was optimized based on Li^+ purity and Li^+ recovery.

CHAPTER 2

LITERATURE REVIEW

2.1. Membrane Separation Process

Membranes serve as barriers that effectively separate two phases within a mixture. They facilitate the separation of substances by permitting certain molecules, ions, or particles to pass through their porous/nonporous structure while blocking undesired substances. Various driving forces, including electrical potential, temperature difference, chemical potential difference, and pressure difference, can be employed for this separation process. The classification of membranes is based on these distinct driving forces that govern the separation mode[11]. Table 2.1 provides a tabulated overview of several membrane processes categorized according to their respective driving forces.

Table 2.1. Driving forces of membrane separation[11].

Driving force	Membrane process	Major applications
Electrical potential	Electrodialysis	Water desalination
Temperature	Membrane distillation	Water desalination
Chemical potential	Pervaporation	Azeotrope separation
	Dialysis	Artificial kidney
	Gas separation	Gas separation
Pressure	Microfiltration (MF)	Water purification
	Ultrafiltration (UF)	Material recovery
	Nanofiltration (NF)	Material recovery
	Reverse osmosis (RO)	Water desalination

Pressure driven membranes are classified as MF, UF, NF, and RO. The main difference among them is the membrane pore size and their respective applications. From

MF to RO membranes, the pore sizes become smaller; thus, the required pressure and energy consumption for separation process increases. Figure 2.1 shows the particle sizes and molecular weight of the components that can be separated by each pressure driven membrane.
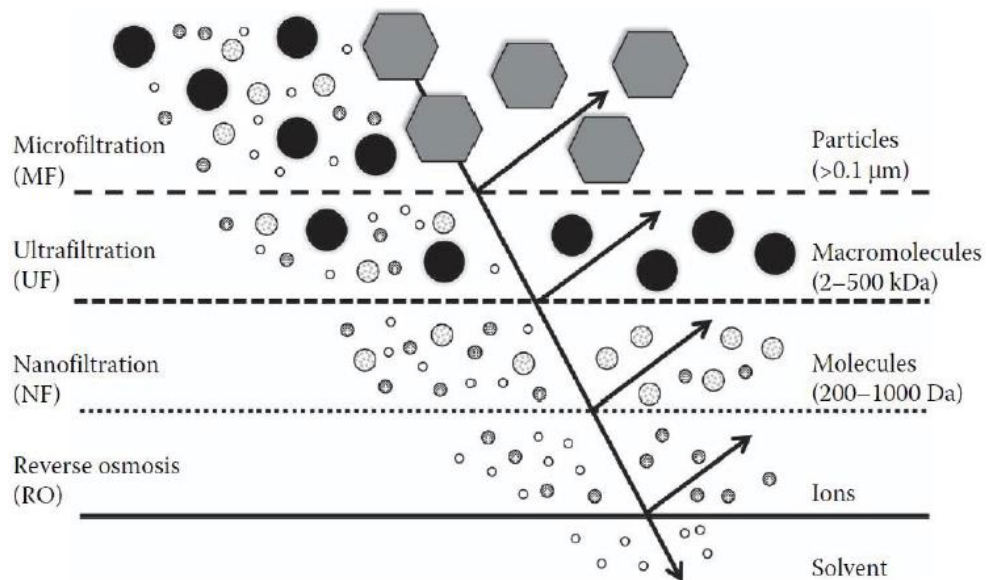
Figure 2.1. Pressure driven membrane separation (Source: taken from Ismail and Jye 2017[12])

After microfiltration, membrane pore size is rated based on filtration capacities. Due to variations in pore size, the molecular weight of solutes that are 90% rejected by the membrane is termed the membrane's Molecular Weight Cut-Off (MWCO). Membrane rejection may vary due to differences in molecule shape and charge. Consequently, MWCO is typically determined by the filtration of non-charged spherical molecules through the membrane. In contrast, the filtration capacities of tight NF (nanofiltration) and RO (reverse osmosis) membranes are significantly influenced by surface charge, and the rejection capacities of these membranes can also be categorized by their salt rejection capacities.

NF is a pressure-driven separation method that selectively separates particles based on size and charge exclusion. The increase in surface charge directly influences the SF [6] due to the Donnan exclusion effect. Two main strategies are typically employed when

creating a surface-charged NF membrane. The first involves the surface polymerization of large pore-sized ultrafiltration (UF)membranes[13–15]. However, modifying commercial UF membranes to produce tight NF membranes can encounter challenges related to pore narrowing due to the interfacial polymerization (IP) mechanism. Researchers have proposed various pore protection strategies to mitigate this effect[16–18]. Additionally, starting with membranes with large pores for the manufacture of NF membranes requires more chemical and energy usage[19], potentially compromising the environmental friendliness and feasibility of the membranes. The second strategy involves modifying tight NF membranes to alter the surface properties of the membranes [20].

2.2. Uses and Sources of Lithium, and Methods for Lithium Extraction

Lithium is one of the critical materials in various industries. In 2016, 35% of the produced lithium was used in battery systems, 32% in the ceramics and glass industry, 9% in lubricating greases, and 24% in other industries [4] . However, in 2022, 74% of the produced lithium was used in battery systems, 14% in the ceramics and glass industry, 3% in lubricating greases, and 9% in other industries [5] (Figure 2.2). These statistics indicate a growing demand for lithium, particularly in applications related to energy storage. Lithium can be produced from a variety of resources, including brine deposits, hard rock minerals, and geothermal brine[6]. Nearly 60% of Li resources are in continental brines and 25% are in hard rocks. According to the U.S. Geological Survey, Mineral Commodity Summaries (January 2021), Australia, the world's largest lithium producer, accounts for 48.7% of total production. They hold 22.3% of the world's lithium reserves, which come from hard rock minerals. On the other hand, Chile, Argentina, and China, with their brine deposit resources (Salt lakes), together constitute 59.8% of total reserves and hold a 46.4% market share (Figure 2.2). The lithium recovery from their salt lakes requires pretreatment processes due to low Li^+ concentrations of the lakes, except Salar de Atacama in Chili and Zabuye in China having high-rich lithium content.
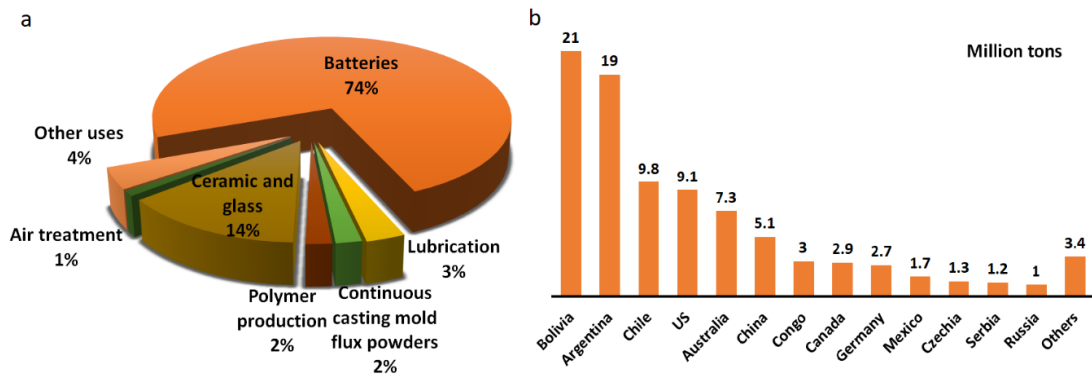
Figure 2.2. a) Lithium resources distribution of global end-use markets, b) Global Li resources distribution[5].

The extraction of lithium brine is commonly applied by pumping it to the surface; and then solar evaporation is applied to the extracted brine. On the other hand, the primary process in extracting lithium from hard rock involves mining and processing lithium-rich minerals. Compared to hard rock lithium extraction, the significant advantages of lithium recovery from brine are as follows: higher initial lithium concentration, lower environmental impacts, cost-effective due to lower energy consumption with using solar evaporation, and scalability. However, the required long production time and large area for solar evaporation process are the challenges for lithium recovery from brine in the conventional method.

Salt lakes contain a variety of salts, such as Na, Mg, Ca, K, Li etc. with different concentrations based on the lake's geological origin. The main challenge for the Li^+ extraction is the low Li^+ concentration and high co-ion concentrations. Among the co-ions, high Mg^{2+} concentration is the key factor determining the Li^+ recovery efficiency. Various methods such as adsorption, solvent extraction, electrochemical, precipitation, and membrane separation, are proposed to extract Li from salt-lake brine. Adsorption is the most commonly used technique in the industry for Li extraction[1]. However, resin regeneration, the capacity, deterioration, and the disposal of used resins limit the practical application of the adsorption, additionally, this process is pH dependent[1]. Solvent extraction techniques generate a high volume of contaminated solvents and impurities, requiring extra treatment and disposal steps, thus increasing environmental impacts, energy consumption and total cost of process [1]. In electrochemical processes, waste stream formation, comprising used electrolytes and electrode components, causes extra

treatment and disposal steps[1] . Processing a large volume of Li-containing solutions by electrochemical methods makes the process even more energy-intensive[1]. The precipitation method for Li purification is a relatively simple operation, cost-effective, and allows to obtain Li with a high purity. However, the main challenge for this method is the presence of Mg^{2+} ions with a significantly higher concentration than Li^+ ions in feed. The Li^+/Mg^{2+} ratio > 6 negatively affects lithium recovery by causing the formation of complex crystalline structure known as $MgCl_2.LiCl.7H_2O$. So, the ratio < 6 is efficient to apply precipitation method [6]. In most salt lakes, the Li^+/Mg^{2+} concentration ratio differs from 1:20 to 1:60 [5]. As a result, the ratio should be decreased < 6 with a preliminary step. Membrane technology is considered promising for obtaining high Li^+ purity and recovery from salt lakes. Desired Li^+ and Mg^{2+} separation is achieved without any chemical reagents resulting in a cost-effective operation.

2.3. Membrane-Based Technologies for Lithium Recovery from Water Lithium Resources

Membrane separation offers selective separation, high efficiency, and scalability. It plays a crucial role in reducing the solar evaporation requirements of Salt Lake brines, which typically need large fields for concentrating salts. Moreover, membranes can be integrated into other processes, contributing to their environmental friendliness [4]. Various membrane separation techniques for Li^+ purification based on different driving forces are outlined below:

1. **Supported Liquid Membranes (SLM):** Utilize chemical potential gradient differences.
2. **Li-Ion Sieve Membranes (LISM):** Rely on concentration differences.
3. **Membrane Distillation Crystallization (MDC):** Operate based on vapor pressure differences.
4. **Ion-Imprinted Membranes (IIM) and Selective Electrodialysis (S-ED):** Employ electrical potential differences.
5. **Permselective Exchange Membrane Capacitive Deionization (PSMCDI):** Utilizes electrostatic adsorption.

6. **Nanofiltration (NF):** Functions based on pressure differences [4].

SLM , prepared by entrapping the liquid in a porous membrane, has shown potential for lithium recovery. They are operated with a low energy consumption and exhibit low fouling tendency. However, they suffer from solvent resistance, stability, and leakage issues [4].

LISM combines the advantages of ion-sieves and membranes, enabling continuous industrial operation. LISM has shown promising adsorption capacity and separation selectivity for lithium recovery. Advantages of LISM membranes are high specific surface area, high selectivity, immobilized sorbents, and low energy consumption. The limitations of LISM are inefficient lithium adsorption/desorption cycle, and low efficiency in lithium recovery [4].

MDC can achieve high concentration factors and recovery. MCD membranes are effective for lithium recovery and water purification, and they have unique mass transfer characteristics. However, the main challenges for the MDC process are fouling, wetting and high energy consumption [4].

IIM combines a porous membrane material with an ion-imprinted polymer, providing the membrane with specific selectivity towards host ions. IIM offers benefits such as specific selectivity, easy regeneration, low energy consumption, increased adsorption capacity, decreased energy consumption, and continuous operation. Disadvantages of IIM membranes are inefficient lithium adsorption/desorption cycle, and low efficiency in lithium recovery [4].

S-ED is an electro-membrane separation process that is widely used in removing salt from water. Advantages of S-ED membranes are low fouling tendency, and potential for process optimization. However, conventional ion exchange membranes used in S-ED cannot effectively separate similarly charged ions, such as lithium and magnesium. In addition, the method is limited to low-to-medium feed salinity and large-scale applications are restricted by excessive costs due to high energy consumption [4]

Figure 2.3 and Figure 2.4 show the energy consumption required for different membrane processes and applicability of these processes. . Each membrane process has its own advantages and limitations, and further research is needed to improve their efficiency, stability, and engineering aspects. Hybrid processes combining Membrane processes with conventional lithium precipitation processes result in higher performance efficiency and reduced cost. When these methods are compared, NF is a promising candidate for Li^+ purification due to moderate energy consumption rate and high

scalability. However, high capital and operating costs restrict the application of the membrane technology. Therefore, in future, module design and process optimization should be further considered to control membrane fouling and membrane stability.
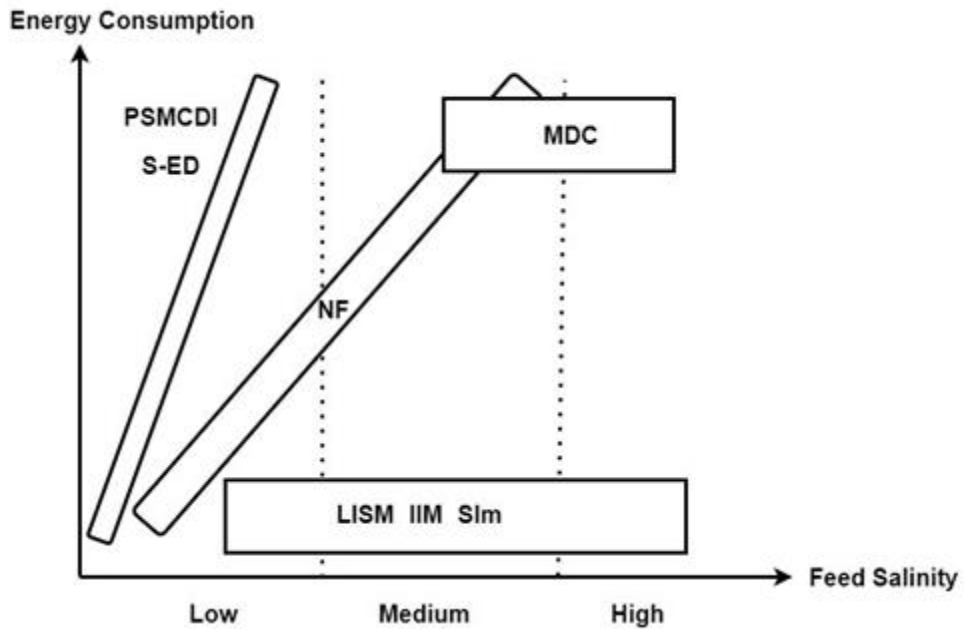
Figure 2.3. Energy consumption rate of different membrane processes [4].
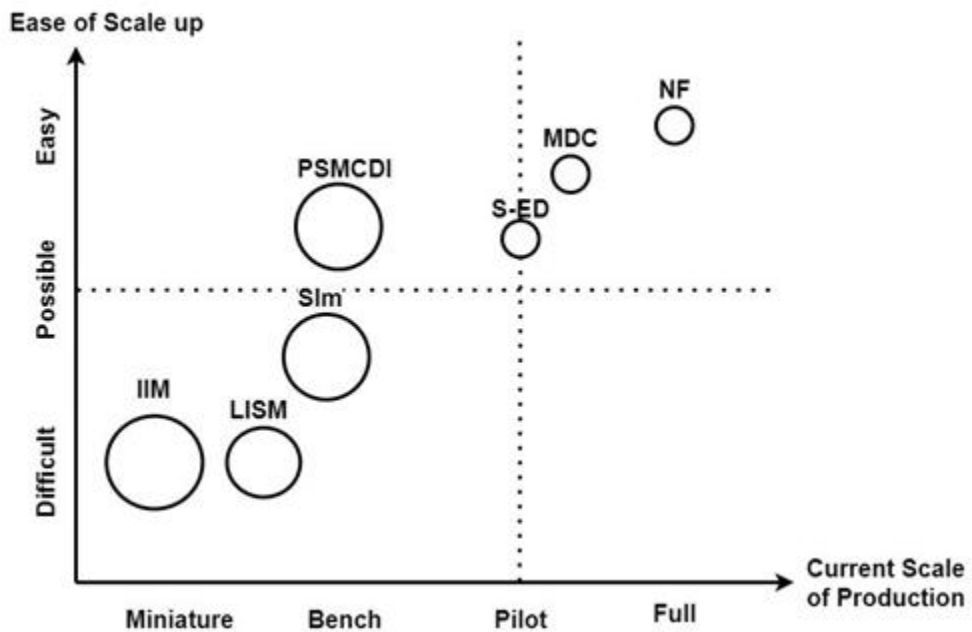
Figure 2.4. Applicability of membrane processes.[4]

11

2.4. Nanofiltration Membranes for Lithium Recovery from Water Lithium Resources

In literature, the first studies about Li^+ and Mg^{2+} separation focused on Polyamide (PA) based commercial thin film composite (TFC) membranes[5]. Yang et al. [21] proposed NF membranes to purify Li^+ and worked on commercial DK membranes. They have defined separation factor as performance criteria. Paramanic et al. [22] studied on commercial NF90 and NF270 membranes integrated with MD system. At optimum conditions of pH 5 and 8 bar, they decreased Mg^{2+}/Li^+ ratio from 10 to 0.19 and 2.1, by NF90 and NF270, respectively while Li^+ rejection was at 77 % and 56 % for NF90 and NF270, respectively. Li et al. [23] worked on commercial DK membranes with high pressure and reported 92% Mg^{2+} rejection at 35 bars. They observed the adverse effect of temperature on the separation factor due to decreased solution viscosity. Additionally, the presence of divalent coexisting ions exerted a significant influence on Li^+ recovery, leading to an increase in the rejection of Mg^{2+} and a decrease in the rejection of Li^+. Sun et al. [24] investigated DL-2540 separation performance with high Mg^{2+}/Li^+ ratio (MLR). They observed that the separation efficiency was negatively influenced by high MLR and increased feed temperature while low pH and high pressure had a positive effect on separation The main drawback of commercial membranes for Li^+ and Mg^{2+} separation is their negative charge, attracting both positively charged Mg^{2+} and Li^+ ions. In addition, the small difference (<0.1 nm) between the hydrated radius of Mg^{2+} and Li^+ ions limit the separation ability of negatively charged commercial membranes. Therefore, many studies focused on developing positively charged NF membranes to benefit from Donnan exclusion effect and they are overviewed in the following sections.

2.4.1. Polyamide (PA) based TFC Membranes

Commercially available polyamide-based membranes have been used in the separation of lithium from brine solutions. However, these membranes have certain

limitations that hinder their performance. One limitation is their small pore sizes, which restrict the flow of water molecules through the membrane. This can result in lower filtration capacities and slower separation rates. Another limitation is related to the negatively charged surfaces of polyamide membranes. While they are effective at repelling negatively charged particles and some larger molecules, they do not provide optimal separation efficiency for positively charged ions like lithium. The repulsive forces between the negatively charged membrane surface and lithium ions are not strong enough to effectively permeate and separate lithium from the brine solution[23,25].

To address these limitations, researchers are exploring various strategies to enhance the performance of polyamide membranes in lithium separation. The strategies applied can be classified into three groups: The interfacial polymerization (IP) regulation, surface functionalization and support modification.

The IP regulation is one of the most effective methods for obtaining target membrane. The surface charge and pore size of the membrane can be changed by adding additives or using new types of monomers. Additionally, specific functional groups, multi amino monomers such as PEI, 1,4-bis(3-aminopropyl) piperazine (BAPP) and nanomaterials are introduced to the aqueous phase during IP reaction to impart positive charge to the surface.

Li et al. published a positively charged PA composite NF membrane. They modified PAN UF hollow fiber membrane with piperazine (BAPP) and trimesoyl chloride (TMC) using IP. The membrane has reached a 2.6 SF while filtering a 2000 ppm salt mixture with a 20 Mg^{2+}/Li^+ ratio. In comparison, the commercial NF90 reduced the ratio from 20:1 to 9.3:1 with $S_{Li/Mg}$ of 2.1 under the same condition. Xu et al. [13] modified a PES membrane by polymerization between PEI and TMC to produce positively charged NF membrane. Membrane had a positive charge below pH 9.3 due to the abundant –NH3 + and –NH2 + groups and reached a $S_{Mg/Li}$ ratio of 0.05 and pure water permeability of 5.02 $L/m^2 \cdot h \cdot bar$ at 8 bar. Wu et al.[18] modified the surface with gas phase amine and TMC at the gas liquid interface and reported the $S_{Li/Mg}$ of 27.38. In addition to the simple IP process, surface polymerization was modified with additives. Aghili et al. [26] have introduced nano gel UiO-66NH2 into PEI TMC IP reaction on PAN membrane. Modified membrane has reached a $S_{Li/Mg}$ of 36.9 with 30.6 $L/m^2 \cdot h \cdot bar$ permeability. Bi et al. [25] published a BAPP/TMC IP reaction modified with carbon nitride functionalized zwitterion molecules. The membrane reached a $S_{Li/Mg}$ of 16-29 during 192 h filtration test. Xu et al.[25] prepared a positively charged PIP-TMC PA layer modified with potassium

carboxylate functionalized multiwalled carbon nano tubes (MWCNTs). The membrane has reached a $S_{Li/Mg}$ of 58 SF with 12.23 L/m^2·h·bar permeability. Hu et al. [27] studied PIP-TMC NF membrane modified with 3,5-bis(sulfinylamino)benzoyl chloride (AB$_2$) and reported a $S_{Li/Mg}$ of 35.7.

Surface functionalization with specific groups or molecules is another effective method for obtaining positively charged NF membrane Lu et al. [28] modified a PIP TMC membrane with PEI 600 and obtained a $S_{Li/Mg}$ of 12.37while filtering salt mixture with a Mg^{2+}/Li$^+$ ratio of 150. Yang et al [29] modified the support membrane with PDA and single-walled carbon nanotubes (SWCNTs). Subsequently, the modified support membrane reacted with PIP TMC to create a selective layer, finally, PEI was introduced with surface grafting. The positively charged NF membrane achieved a $S_{Li/Mg}$ of 33.4. Luo et al. [30] used a novel monomer 1- (2-hydroxyethyl)-1,3,5,7-tetraazaadamantane-1-ium bromide (HMTAB)which was attached to the PEI composite membrane through esterification condensation. The looser structure of the membrane resulted in a high permeability (16.3 L/m^2·h·bar) with a $S_{Li/Mg}$ of 10.1 after 25 h's continuous operation. Feng et al [31] functionalized the PEI NF membrane with quaternized bipyridine (QBPD) grafting. QBPD increased membrane permeability nearly three times and compared to the commercial membranes, resulted in relatively higher $S_{Li/Mg}$. of 5.2 and permeability (16.6 L/m^2·h·bar). Xu et al. functionalized the PEI TMC surface with N,N,N',N'-tetrakis (2-hydroxypropyl) ethylenediamine (QEDTP). QEDTP membrane had a $S_{Li/Mg}$ of 15.6 with 18.8 L/m^2·h·bar permeability. Wu et al. functionalized the PIP TMC membranes with 1-(3-aminopropyl)-3-methylimidazolium bis(trifluoromethanesulfonyl) imide ([MimAP][Tf2N]) grafting. The membrane had a $S_{Li/Mg}$ of 8.12. The y, commercial NF membranes, DL, NF270, DK, were functionalized with PDA and PEI grafting. Prepared membranes reached the $S_{Li/Mg}$ of 5.1, 7.2 and 59.5 SF respectively [20].

Substrate modification is also applied to adjust the Li$^+$/Mg^{2+} separation properties of the membranes. For example, Xu et al.[32] applied IP of PEI and TMC on PES UF membrane blended with GO. Guo et al.[14] immersed the PES substrate membrane into the mixed solution of polydimethyl diallyl ammonium chloride (PDDA) and NaCl and then attached a carboxylated cellulose nanocrystal (CNC-COOH) interlayer and finally formed the thin PEI-TMC PA layer. Xu et al.[33]modified the PES support with MWCNTs-COOK and then formed the PEI-TMC NF membrane on this support.

2.4.2. Other NF Membranes

Although PA based IP process is the dominant method in developing NF membranes, other techniques have also been applied. The most commonly used technique is layer by layer (LbL) surface modification. Wang et al [34] synthesized Cu coordinated m-phenyl-enediamine (MPD) membrane on a PES support, and then crosslinked it with glutaraldehyde (GA). Cu-MPD membrane achieved a $S_{Li/Mg}$ of 8 with 16.2 $L/m^2 \cdot h \cdot bar$ permeability. Yang et al.[35] studied LbL surface modification of polyallylamine hydrochloride (PAH), DA and poly (sodium 4-styrenesulfonate) (PSS).PAH/DA/PSS membrane reached to $S_{Li/Mg}$ of 37.8 with 21.9 $L/m^2 \cdot h \cdot bar$ permeability. He et al [36] produced a PSS/PAH hollow fiber NF membrane with multiple layers. After 2.5[th] bilayer, the coating on PES membrane was crosslinked by GA. PSS/PAH membrane reached the $S_{Li/Mg}$ of 75and 18.4 $L/m^2 \cdot h \cdot bar$ permeability.

2.5. Nanofiltration Separation Mechanisms

Nanofiltration, which sits at the center of ultrafiltration and reverse osmosis, is a membrane-based separation process distinguished by its selectivity on solute passage. The NF membrane exhibits a nominal molecular weight cutoff within the 100–1000 Da range, suggesting that its active layer has pores of approximately 1 nm in size. The separation of solutes within the NF range relies on micro-hydrodynamics and interfacial events at both the membrane surface and within the membrane itself. Rejection of solutes is controlled by steric and non-steric effects[37–39].
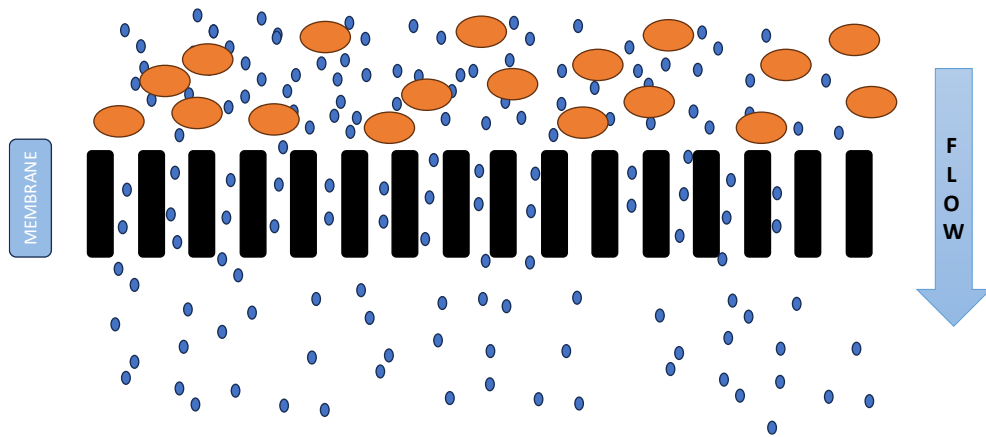
Figure 2.5. Size exclusion mechanism

Size exclusion is the core principle of nanofiltration, which operates through small pores in the fabric of membranes that have been specifically designed. These pores, use accurate molecular sieving, allowing small ions and molecules in while successfully rejecting larger molecules (Figure 2.5). This strategy highlights the crucial role of designed membrane engineering for succeeding in targeted molecule separation. The retention of neutral solutes is only possible with the size exclusion mechanism.

The Donnan exclusion principle is based on interaction of ions in solution with the charges on the membrane surface. In NF, the membrane is often produced with a surface charge, either positive or negative. This charge is caused by the dissociation of functional groups on the membrane material, which makes it electrostatically active. Consider the instance where the NF membrane has a net negative charge. According to the Donnan exclusion principle, this negatively charged membrane preferentially attracts and repels ions in the bulk phase. Positively charged ions (cations) will be permeated to the negatively charged membrane, whereas negatively charged ions (anions) will be repelled (Figure 2.6).
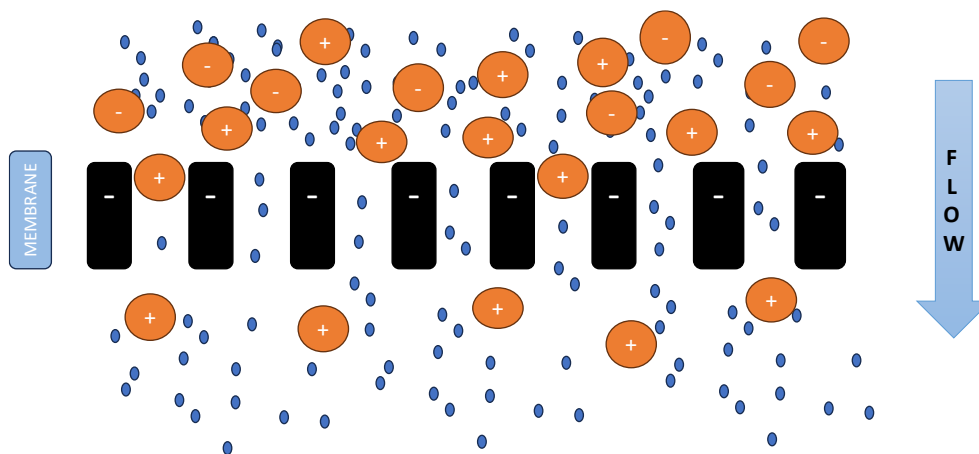
Figure 2.6. Donnan exclusion mechanism

The mechanism of Dielectric Exclusion discusses the extensive interactions between solute and solvent in the membrane matrix. This mechanism is modulated by the dielectric properties of the membrane material. In order to gain a quantitative understanding of these interactions and to provide additional insight into the different affinities of solutes and solvents with the membrane matrix, mathematical models are deployed.

Another important mechanism that controls the solute rejection by NF membranes is dielectric exclusion (Figure 2.7). In dielectric exclusion mechanism, the energy barrier resulting from the shedding of the hydration shell becomes a challenge for the solute in penetrating the membrane[40]. Specifically, when ions pass through the membrane via pores equal to or smaller than their hydrated size, dehydration becomes a necessary step[41,42]. According to the ion dehydration theory, a lower ion hydration energy can enhance steric exclusion[43,44]. This enhancement occurs because, in such instances, the water shells enveloping the ion are easily stripped away during the membrane passage[45–47]. Notably, in contrast to the Donnan effect, it has been claimed that the dielectric exclusion mechanism is independent of the ion's sign[41].
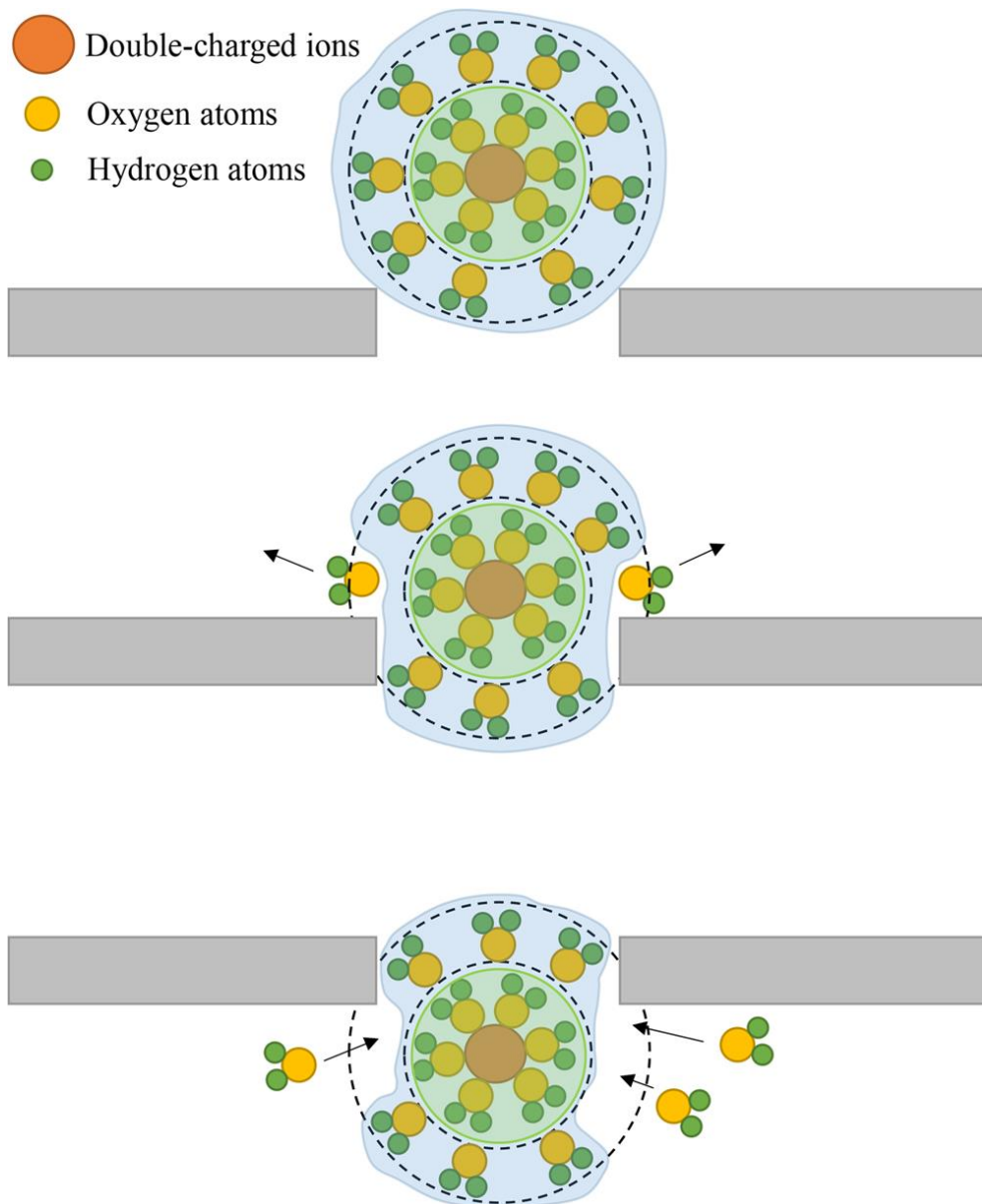
Figure 2.7. Dielectric exclusion mechanism (Source: taken from Chen et al. 2017[48])

Various models based on Extended Nernst–Planck equation is used to describe transport through NF membranes is described by NF models based on the. Among these models, the most commonly used one is the Donnan-Steric partitioning Pore Model (DSPM) developed by Bowen et al.[49]. In DSPM, solute transfer occurs through the following steps: 1) Distribution of charged species at the membrane–solution interface due to both size exclusion and Donnan exclusion. 2)Transfer through the membrane as a result of convection, diffusion, and migration. Later on, Szymczyk and Fievet [50] improved DSPM by including the dielectric exclusion mechanism. Considering all three rejection

mechanism, the equilibrium partitioning of a solute between the bulk and the NF membrane is described by the following equation[51]

$$\frac{\gamma_i c_i}{\gamma_i^0 C_i} = \Phi_i \exp\left(-\frac{z_i F}{RT}\Delta\psi_D\right) exp\left(-\frac{\Delta W_i}{k_B T}\right) \qquad (2.1)$$

where c_i and C_i are the concentrations at the membrane interface and in the bulk, γ_i and γ_i^o represent activity coefficients, Φ_i is the steric rejection parameter, k is the Boltzmann constant, T is the temperature, z is the ion valence, ψ the mean potential and W_i the interaction free energy including all interactions of the ion with the medium. In Equation 2.1 the Donnan term is represented by the first exponential term while the dielectric contribution is shown by the second exponential term.

Ion solvation energy barrier, ΔW, described from Born model is expressed as[51]

$$\Delta W_i = \frac{z_i^2 e^2}{8\pi\varepsilon_0 a_i}\left(\frac{1}{\varepsilon_p} - \frac{1}{\varepsilon_b}\right) \qquad (2.2)$$

where, a_i is the solute hydrodynamic radius (Stokes Radius), e is the elemental electron charge, ε_o, ε_p and ε_b are the permittivity of free space, the pore dielectric constant and the bulk dielectric constant, respectively.

In summary, size exclusion, the Donnan effect, and dielectric exclusion are combined to create an effective membrane-based filtration system. Mathematical models are beneficial for the quantitative understanding and process optimization of NF, particularly in the context of dielectric exclusion. This thesis points out the complexity of these mechanisms, thus defining NF as a vital and adaptable instrument for a wide range of industrial and environmental applications.

CHAPTER 3

MATERIALS AND METHODS

3.1. Materials

PAI (Solvay Advanced Polymers, trade name Torlon, 4000T-LV), N-methyl-2-pyrrolidone (Merck, NMP, anhydrous, > 99.5%), branched PEI (Sigma Aldrich, 25kDa), and 1,4-dioxane (Merck) were used for support membrane production. Al(III)O (Riedel), DA (Sigma Aldrich), tris hydrochloride buffer (Sigma Aldrich) and PEI (Sigma Aldrich, 800Da) were used for membrane surface modification. $MgCl_2$ (Afg Bioscience), LiCl (Carlo Erba), glucose (Merck), sucrose (Sigma-Aldrich), PEG 400, 600, 1000, 4000, and 6000 Da provided by Sigma Aldrich were used for the membrane rejection tests. Sodium hydroxide (Sigma Aldrich, 98% purity) was used for pH adjustment. All solutions were prepared by using ultra-pure water (conductivity<0.055 us/cm).

3.2. Membrane Preparation

3.2.1. Preparation of Support Membranes by Phase Inversion Method

PAI-based support membranes were prepared by the phase inversion method. First, PAI was dried in a vacuum oven at 177°C for 3h to remove moisture and was dissolved (15, 17, or 20 wt.%) in a dioxane: NMP (1:3, 1:5, or 1:7 wt. ratio) mixture. The mixture was stirred at 70°C for 18h until a homogeneous solution was obtained, and stirring was stopped to eliminate air bubbles. The prepared casting solution was spread on a polyethylene terephthalate nonwoven fabric (Type 2413 Novatexx, Freudenberg Filtration Technologies India Pvt. Ltd.) with the help of an automated film applicator (Sheen Instrument Ltd., model number: 1133N). The initial wet thickness of the cast

membrane was adjusted to 150, 200, or 250 μm. The casted film was immersed into a 2L ultra-pure water coagulation bath with/without 0.5 w.% PEI for 36 h. Finally, the prepared membranes were rinsed with ultra-pure water and stored in ultra-pure water for surface modifications at room temperature. The membranes were coded as PAI membrane when coagulation bath including only water and PEI-PAI membrane when coagulation bath including 0.5 w.% PEI in water.

3.2.2. Preparation of Polydopamine Coated PEI-PAI Membranes (PDA/PEI-PAI Membranes)

PDA modification onto the PEI-PAI support membrane was applied using a custom-designed coating device (Figure 3.1) adapted from the study of Dobosz et al.[17]. 50 mL of 10mM Tris-HCl reaction solution at a pH of 8.5 was poured onto the active side of the membranes. Then, DA (2 mg/mL) was added to the reaction medium while shaking at 100 rpm. O_2 gas flow was continuously applied from the more porous surface of the membrane at 0.2 bar to prevent polymerization inside the pores and enhance the polymerization rate. Polymerization was stopped at the end of the 10, 20, or 40 min. The membranes were washed with ultra-pure water to remove unreacted monomers from the membrane surface. The PDA-coated PEI-PAI membranes were named PDA/PEI-PAI membranes.
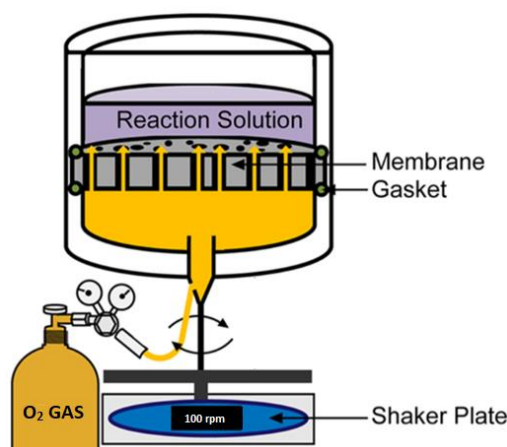
Figure 3.1. Experimental setup used for in-situ dopamine polymerization.

3.2.3. Preparation of PEI Functionalized Alumina Immobilized PDA/PEI-PAI Membranes (Al/PDA/PEI-PAI Membranes)

Alumina particles were functionalized with PEI (25 kDa) to achieve chemical stability and higher positive charge density in the membrane surface before immobilization of alumina onto the PDA/PEI-PAI membrane.

3.2.3.1. Ball Milling Process for Alumina Particles

Alumina particles in water were grinded with a plenary ball mill (Retsch PM 100) for 48 h to obtain nanometer-sized particles, increasing the homogeneity of particles coating on the membrane surface and effective surface area. The particle size distributions were determined by using the NanoPlus8 Micromeritics Instrument.

3.2.3.2. PEI Functionalization of Alumina Nanoparticles

Alumina nanoparticles were functionalized using PEI (25 kDa) using the procedure adapted from [52] Firstly, 0.5 g of alumina nanoparticles were dispersed in 15 mL methanol using an ultrasonic bath at room temperature for 10 min. PEI (25 kDa) was added at different concentrations (5, 10, 15, 20 and 30 mg/mL). The reaction occurred at a constant stirring (400 rpm) for different reaction periods (3, 6, and 9 h) at 50°C. The volatile components of the mixture were condensed back using a condenser, and the powder was subjected to three methanol washes to eliminate any remaining unreacted chemicals. The particle size distributions and zeta potentials of PEI functionalized alumina nanoparticles were determined using the NanoPlus Micromeritics Instrument.

3.2.3.3. Immobilization of PEI Functionalized Alumina onto PDA/PEI-PAI Membranes

For immobilization of PEI-functionalized alumina particles onto the membrane surface, 0.01wt.% alumina in water at different volumes (13.1, 26.2, 52.3, and 78.4 L/m^2) were filtered through the PDA/PEI-PAI membranes at 2.5 bar. After filtration, membranes were backwashed with ultra-pure water to remove loosely bound particles from the membrane surface. These membranes were coded as Al/PDA/PEI-PAI membranes.

3.2.4. Preparation of PEI Coated Al/PDA/PEI/PAI Membranes (PEI/Al/PDA/PEI-PAI)

For PEI modification on Al/PDA/PEI-PAI membrane, 20g/L PEI (800 Da) aqueous solution at different volumes (3.5, 7.0, and 10.5 L/m^2) was filtered through the Al/PDA/PEI/PAI membranes at 2.5 bar. Then, the membranes were backwashed with ultra-pure water to remove unbounded compounds. These membranes were coded as PEI/Al/PDA/PEI-PAI membranes.

Figure 3.2 illustrates the final membrane structure, showcasing the deposition of each layer on top of one another.
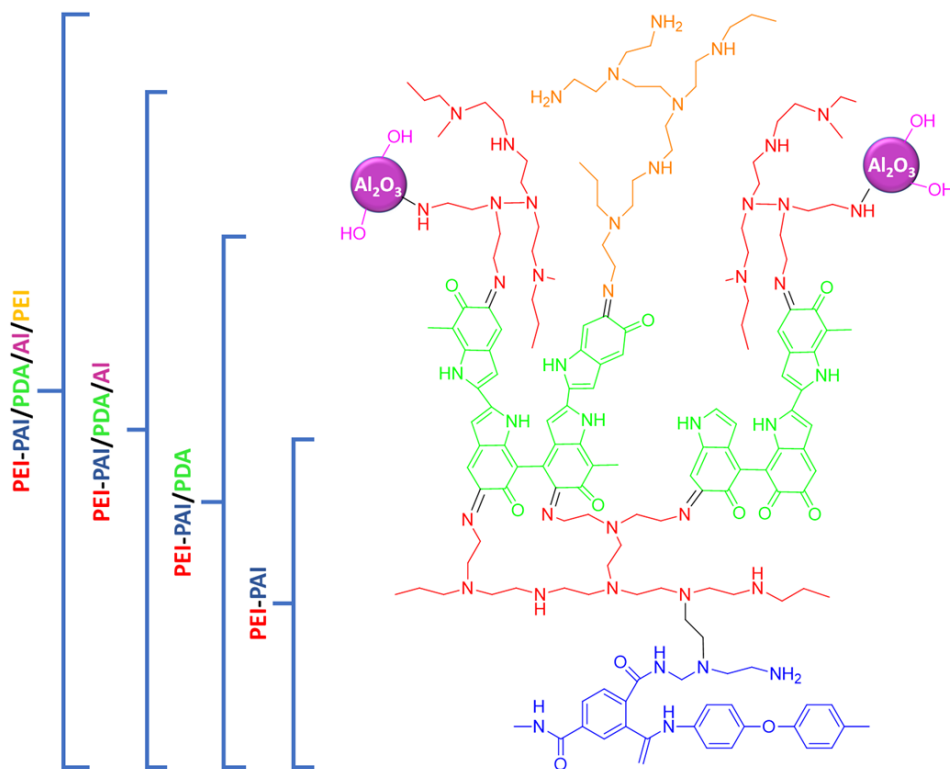
Figure 3.2. The proposed binding mechanism between PDA/PEI-PAI and PDA-Alumina Nanoparticles and PDA-PEI.

3.3. Performance Tests of the Membranes

The filtration performance tests were conducted with a dead-end filtration stirred cell (Millipore, Amicon Stirred Cell 200mL, active membrane area: 28.7 cm^2). Each membrane was compacted at 4 bars until reaching steady-state conditions. After that, pure water permeability (PWP) was calculated by using the equation below.

$$PWP = \frac{\Delta V}{A \Delta t \Delta P} \tag{3.1}$$

where, ΔV is the volume of permeated water(L), A is active membrane area, Δt is permeation time (h), ΔP is transmembrane pressure difference (bar).

The rejection levels of the PEG (1000, 4000 and 6000 Da) aqueous solutions for the PAI, PEI-PAI, and PDA/PEI-PAI membranes were determined by filtering 1 g/L PEG solutions through the membrane at 1 bar under 300 rpm constant stirring rate The concentrations of PEG in permeate, retentate and feed solutions were measured by using Rudolph - J357 Automatic Refractometer. Single ($MgCl_2$) salt rejection performance of the Al/PDA/PEI-PAI and PEI/Al/PDA/PEI-PDA membranes was tested by filtering 2000 ppm $MgCl_2$ solution at 3 bars. The concentration of $MgCl_2$ in feed, permeate and retentate streams were measured by Hach HQ 4300 conductometer. The 2000 ppm LiCl : $MgCl_2$ salt mixture with a 1:20 Li^+:Mg^{2+} ion mass ratio was also filtered through the PEI/Al/PDA/PEI-PAI membranes to determine selectivity of the membrane. . The concentration of LiCl and $MgCl_2$ in feed, permeate and retentate streams were measured using the inductively coupled plasma optical emission spectrometry (ICP-OES, Agilent 5110). The PEG and salt rejections of the membranes were calculated from Eq. 3.2 while the separation factor ($SF_{Li,Mg}$) for the PEI/Al/PDA/PEI-PDA membranes was calculated using Eq. 3.3.

$$R(\%) = \left\{ 1 - \frac{C_P}{\frac{C_F + C_R}{2}} \right\} \times 100 \qquad (3.2)$$

where C_F, C_P, and C_R are the concentrations of solutes in feed, permeate, and retentate, respectively.

$$SF_{Li,Mg} = \frac{C_{Li,p} / C_{Mg,p}}{C_{Li,f} / C_{Mg,f}} \qquad (3.3)$$

and $C_{Li,p}$ and $C_{Mg,p}$ are the Li^+ and Mg^{2+} concentrations in permeate, and $C_{Li,f}$ and $C_{Mg,f}$ are the Li^+ and Mg^{2+} concentrations in feed solution, respectively.

3.4. Characterization of the Membranes

The surface morphology of each layer of the optimum PEI/Al/PDA/PEI-PAI membrane was observed using a scanning electron microscope (SEM) (FEI Quanta 250 FEG). Before taking images, the membranes were fractured in liquid nitrogen and coated with gold. Elemental mapping analysis was conducted to assess the homogeneity of membrane coatings using Energy-Dispersive X-ray Spectroscopy (EDX) on ZEISS EVO10. Atomic force microscopy (AFM, MMSPM Nanoscope 8 Bruker) was used to measure the roughness of the membrane surface by taking topographic images of 5 μm × 5 μm-sized dried membrane surfaces at a rate of 1 Hz. The membranes' zeta potentials were measured in 10 mM NaCl solution at pH 7 using NanoPlus Micromeritics Instrument. The water contact angles of the dried membranes were measured with 5 μL of a deionized water droplet to determine the hydrophilicity of the membrane.

3.5. Stability of PEI/Al/PDA/PEI-PAI Membrane

The stability of the optimum PEI/Al/PDA/PEI-PAI membrane was evaluated by measuring the amounts of alumina nanoparticles released into the 2000 ppm $LiCl : MgCl_2$ salt mixture ($Li^+:Mg^{2+}$ ratio 1:20) at the end of 1, 3, 5, 7, 15, and 30 days of storage. Additionally, the PWP and salt rejections of the stored membrane were determined. The released amounts of nanoparticles were determined using ICP/OES.

Furthermore, the membrane stability was dynamically tested by filtering a 2000 ppm salt mixture for up to 72 hours. After 5% of the salt mixture was filtered, permeate solution was loaded into the reservoir to eliminate osmotic pressure buildup. During filtration, permeate and retentate samples were collected every hour, fresh salt solution at the same volume as the collected permeate was loaded into the reservoir; additionally, solute permeability was recorded to observe the fouling tendency of the membrane.

CHAPTER 4

RESULTS AND DISCUSSION

4.1. Membrane Preparation

Separating lithium and magnesium ions requires a membrane in the nanofiltration category. Although single-step membrane preparation is always preferred due to simplicity, reaching both desired membrane properties, such as surface charge, hydrophilicity, and pore size, can be a challenge. In this case, multistep preparation becomes necessary, and the LbL membrane modification method is an excellent alternative. In this thesis, the membrane preparation can be classified under four steps. The first step is to form a suitable porous substrate; the second step is to create an intermediate layer to make a bridge between the support and the outermost layer; and finally, the third and fourth steps attach and impregnate positively charged groups on the surface.

4.1.1. Preparation of Support Membranes by Phase Inversion Method

The number of layers in preparing the NF membranes is critical and depends on the pore size of the substrate. In literature, generally, commercial UF membranes with a molecular weight cutoff value above 30 kDa are used as support [18,33–35,53,54] ; however, such supports require depositing many layers of polymers and nanoparticles to obtain the pore size of an NF membrane, leading to a high chemical and energy consumption. Therefore, it is beneficial to prepare a support membrane with a much smaller pore size to limit the number of layer depositions on the support. Indeed, a support membrane in the tight UF category is needed for further surface modifications, to prepare such a support, polymer concentration, membrane thickness, and co-solvent ratio were varied during casting of the membrane-forming solutions.
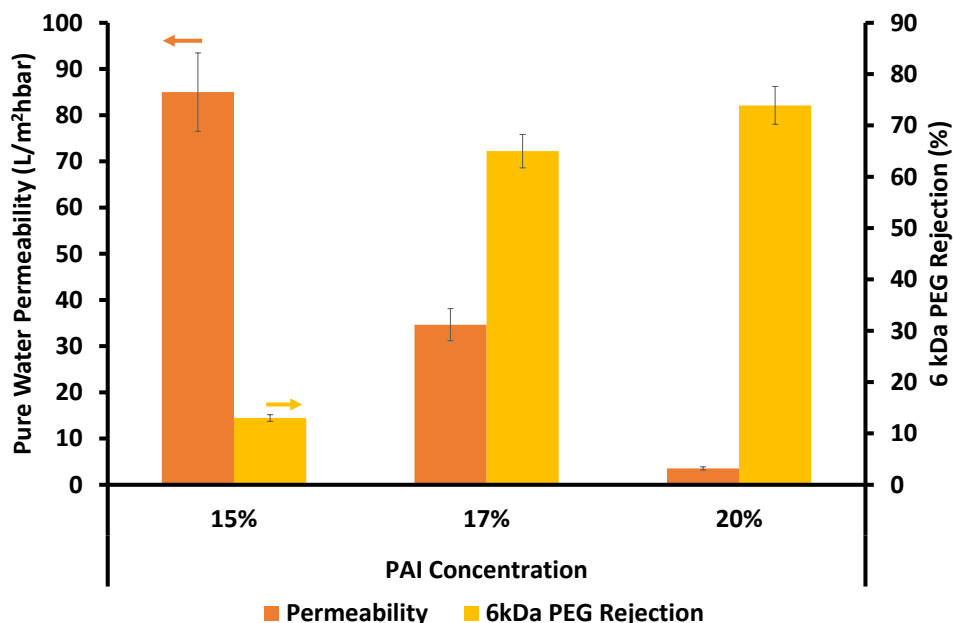
Figure 4.1. The effect of polymer concentration on the pure water permeability and PEG 6 kDa rejection of the membranes. The casting thickness: 200 μm and Co-solvent content: 0%.

As it is known, there is a trade-off between pure water permeability and the rejection capacity of the membrane. Although high permeability is desirable, the challenge is the similar particle sizes of Li^+ and Mg^{2+} ions. Therefore, the rejection capacity of the membrane for PEG 6 kDa and PEG 1 kDa was chosen as the main criteria for selecting the optimum support membrane preparation conditions. Figure 4.1 illustrates how varying polymer concentration influences both the PWP and rejection of PEG 6 kDa in membranes cast with a wet thickness of 200 μm without using a co-solvent in the casting solution. As the polymer concentration increased from 15% to 20%, the PWP decreased from 85 to 3.5 L/m²·h·bar, while the PEG 6 kDa rejection value exhibited an incredible increase, rising from 13% to 74%. The transition from 15% to 17% in polymer content resulted in a notable 2.5-fold reduction in PWP but a fivefold enhancement in rejection. Conversely, further elevating the polymer concentration from 17% to 20% led to a significant PWP decline, coupled with a negligible improvement in PEG 6 kDa rejection.
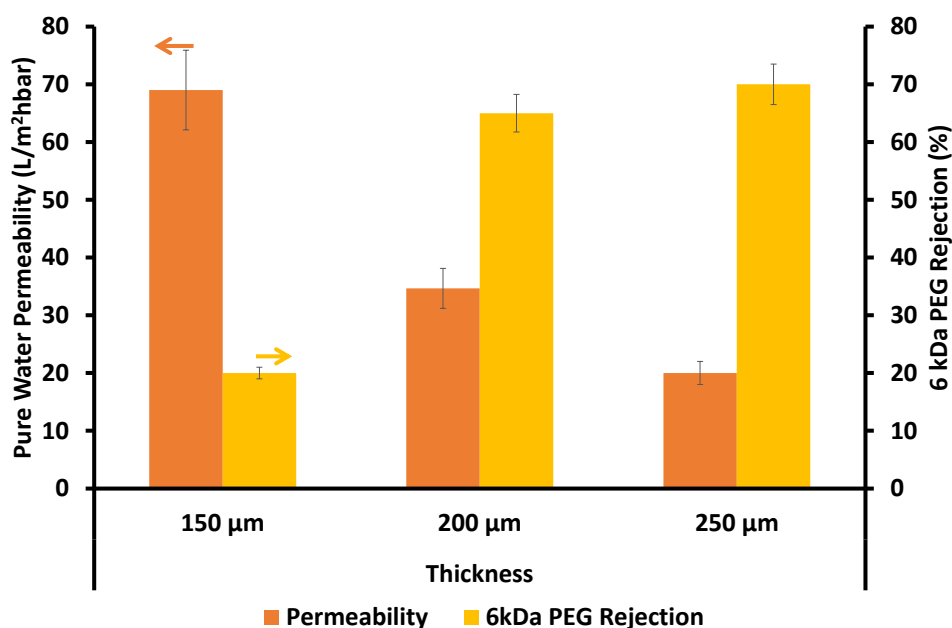
Figure 4.2. The effect of wet casting thickness on the pure water permeability and PEG 6 kDa rejection of the membranes. The PAI concentration: 17%   and Co-solvent content: 0%.

Consequently, the optimal polymer concentration was Figure 4.2 shows the effect of the wet casting thickness on the PWP and PEG 6 kDa rejection values for the membranes prepared with 17 % polymer content without using a co-solvent. Casting the membrane with 150 μm wet thickness provided a high PWP (69 L/m^2·h·bar), but the PEG 6 kDa was too low (20 %). The membranes, prepared with 200 and 250 μm casting thicknesses, gave similar PEG 6 kDa rejection values (65 % and 70 %); however, the PWP was higher when the casting thickness was 200 μm (35 L/m^2·h·bar and 20 L/m^2·h·bar for 250 μm). As a result, the optimum casting thickness was selected as 200 μm.
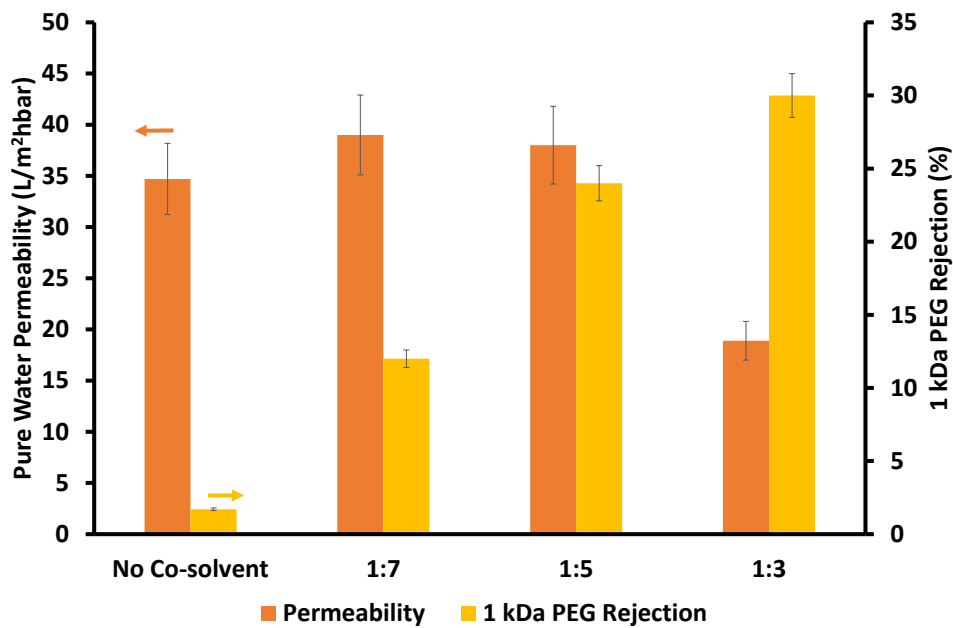
Figure 4.3. The effect of co-solvent ratio on the pure water permeability and PEG 1 kDa rejection of the membranes. The PAI concentration: 17% and casting thickness: 200 µm.

To further reduce the pore size of the support membrane, dioxane was added as a cosolvent into the casting solution at three different compositions. Figure 4.3 illustrates that a cosolvent addition can significantly influence membrane permeability and rejection characteristics. The membrane prepared using only NMP rejected 1 kDa PEG at 3%. However, increasing the Dioxane: NMP ratio from 1:7 to 1:3 improved the rejection of PEG 1kDa from 12% to 30%, concurrently reducing permeability from 39 to 18.9 L/m²·h·bar. The membranes prepared with the Dioxane: NMP ratio of 1:5 and 1:7 had statistically insignificant PWP and PEG 1 kDa rejections; thus, the optimum Dioxane: NMP ratio was set to 1:5. Dioxane cannot completely dissolve the PAI since its solubility parameter, 20.4 MPa$^{0.5}$ [55], is lower than PAI's, 23 MPa$^{0.5}$ [56]. In contrast, NMP, with an equivalent solubility parameter of PAI, [57] is an excellent solvent for PAI. Adding dioxane reduced the affinity between the solvents and the PAI and increased the casting solution's viscosity. As a result, the exchange rate of mixed solvents with water decreased, leading to a smaller pore size on the surface. The last strategy applied to reduce the pore size of the support further was to add 5 g/L PEI into the coagulation bath. The PEI addition did not decrease the PWP of the support while increasing the PEG 1 kDa rejection from 24% to 77%. Based on the results presented in Figure 4.1 through Figure 4.3, the support

preparation conditions were set as follows: 17% PAI content, a 1:5 Dioxane: NMP ratio, a casting thickness of 200 μm, and a coagulation medium of water containing 5 g/L PEI.

4.1.2. Preparation of Polydopamine Coated PEI-PAI Membranes (PDA/PEI-PAI Membranes)

Polydopamine has gained attention as an intermediate layer in various surface modification processes due to its ability to adhere to multiple surfaces in wet environments. The primary amine and catechol groups in the dopamine structure allow for the attachment of positively charged particles and groups. Thus, the PAI-PEI support membrane was first coated with dopamine at three coating times.

SEM and EDX images of support and PDA-coated membranes are given in Figure 4.4 Figure 4.5 , respectively. Both images show uniform elemental distributions. After modification of the support membrane, the O_2 amount increased from 22.74% to 23.51%, which confirmed the presence of the PDA layer (Table 4.1).
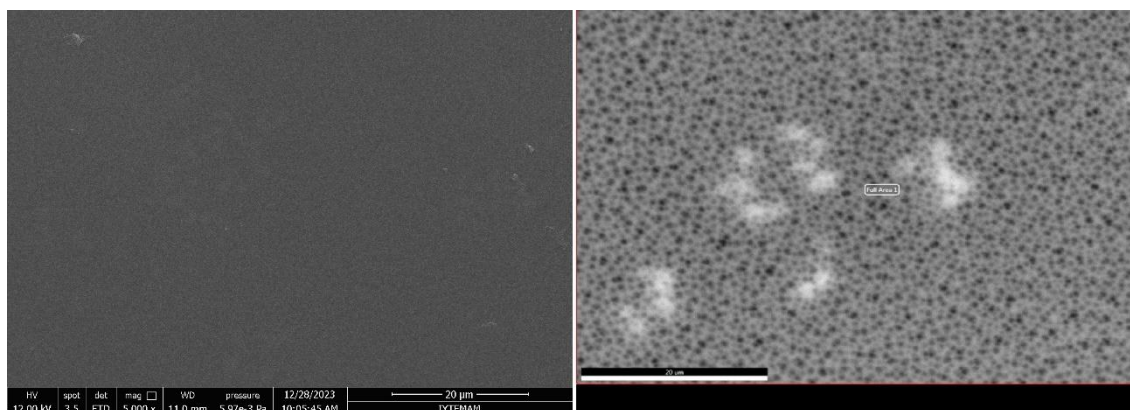
Figure 4.4. SEM and EDX images of support membrane.
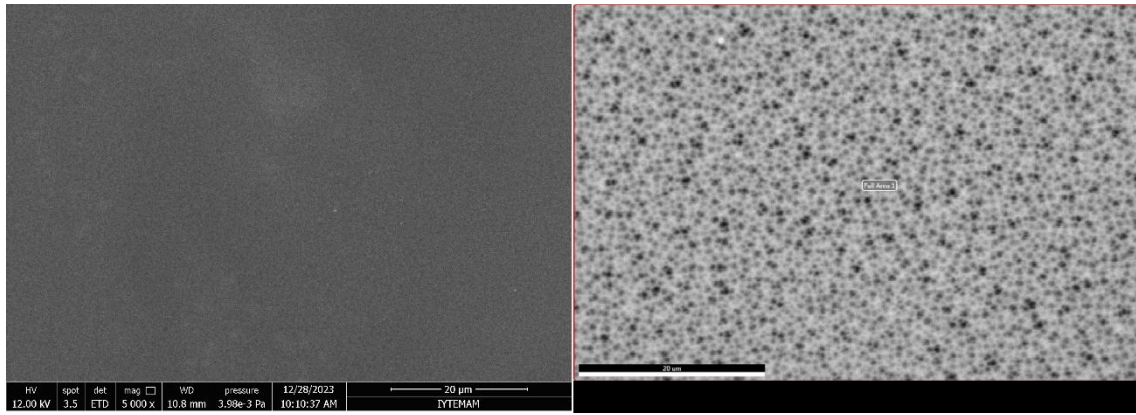
Figure 4.5. SEM and EDX images of the PDA coated PEI-PAI membrane.

Table 4.1. Elemental analysis of the support and PDA coated PEI- PAI membrane.

Element	PEI-PAI (wt.%)	PDA/PEI-PAI (wt.%)
C	57.88	55.72
N	19.38	20.76
O	22.74	23.51
Total:	**100.00**	**100.00**

Figure 4.6 presents the AFM images of the support, and PDA coated support membranes. The PDA layer improved the roughness of the PEI-PAI membrane, most probably due to short-chained PDA filling the valleys created by long-chained PEI.
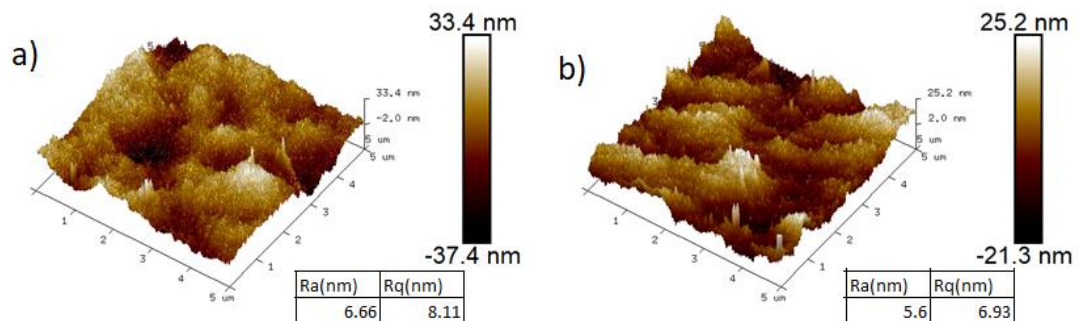
Figure 4.6. AFM images of a) support and b) PDA coated PEI-PAI membranes.

The effect of coating time on the performance was evaluated based on the change in the pure water permeability and PEG 1 kDa rejection after coating.
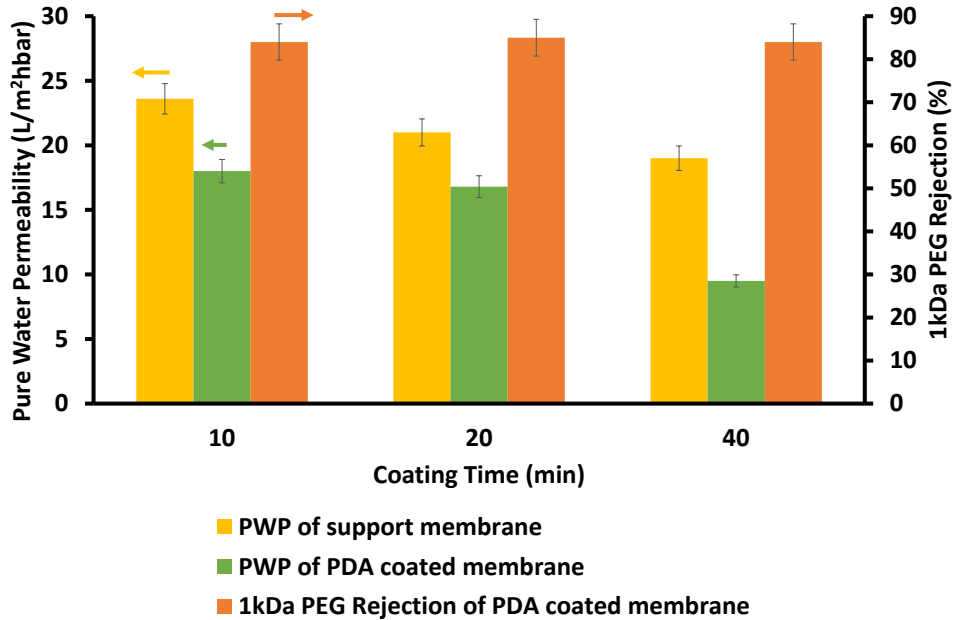
Figure 4.7. The effect of PDA coating time on the pure water permeability and 1kDa PEG rejection of the coated membranes

Figure 4.7 illustrates that the dopamine coating enhanced the PEG 1 kDa rejection from 77% to 85% regardless of the coating time. In contrast, a 40-minute dopamine polymerization reduced the pure water permeability by 50%, while the decline for 20 and 10-minute polymerization was 20%. PDA layer is an intermediate layer for other layers. Since the performance of these two conditions were found as similar, increasing the open-ends of PDA molecules, that could bond with other layers, would be improved the separation efficiency of the final membrane. Based on these results, dopamine coating time was chosen as 20 minutes. The PDA-coated membrane rejected Mg^{2+} at 37 %.

4.1.3. Preparation of PEI Functionalized Alumina Immobilized onto PDA/PEI-PAI Membranes (Al/PDA/PEI-PAI Membranes)

Following the polydopamine coating, the pore size remained excessively large, and the insufficient Mg^{2+} rejection indicated the need for additional layers. For LbL assembly, the purpose was to improve the Mg^{2+} rejection without significantly decreasing the flux. Thus, low molecular weight PEI (800 Da) was assembled on the PDA layer, and the Mg^{2+} rejection increased from 37 % to 63 %, which was still low. Incorporating nanoparticles into the LbL assembly enhances its hydrophilicity, permeability, selectivity, and mechanical properties. To this end, the dopamine-modified support was coated with Al_2O_3 since the metal oxides have a high capacity to form coordination bonds with polydopamine. Before coating, the particle sizes of alumina were decreased from 2.68 μm to 250 nm with ball milling within 48 h. Al_2O_3 coating on the polydopamine-coated layer increased the Mg^{2+} rejection from 49.4% to 63.6% while reducing the pure water permeability from 21.2 to 9.3 $L/m^2 \cdot h \cdot bar$. However, the Al_2O_3 particles were unstable on the membrane surface after the membrane was immersed in a 2000 ppm aqueous salt solution containing Li^+ and Mg^{2+} with a Li^+: Mg^{2+} ratio of 5. Then, to facilitate the stability of the alumina particles in the salt environment, they were coated with 25 kDa of PEI. Reaction time and PEI concentration were optimized based on the change in particle size and zeta potential of particles after modification.
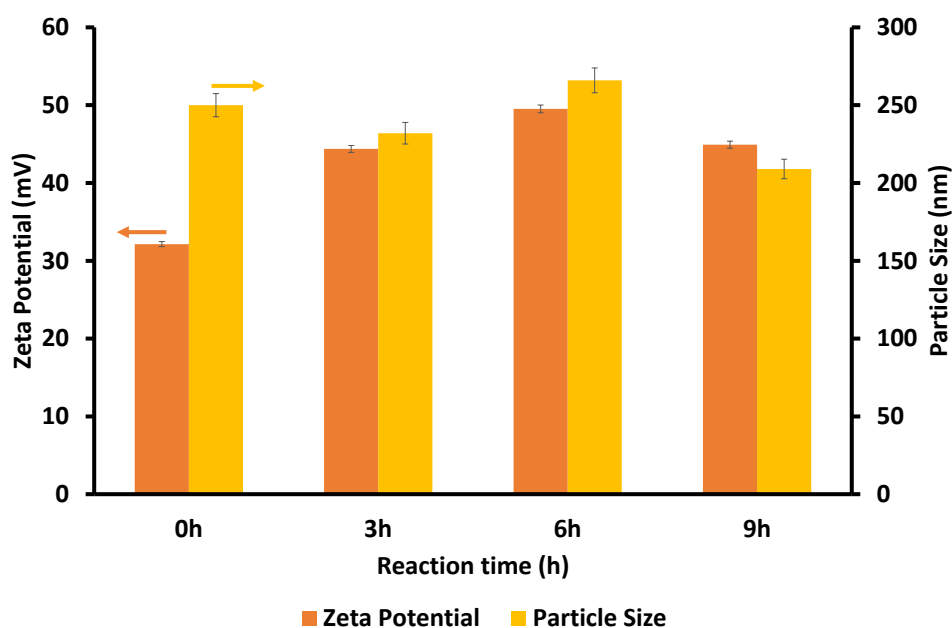
Figure 4.8. The effect of coating time on the particle size and zeta potential of the PEI-coated Al_2O_3 particles. PEI concentration: 10 wt. %

At first, alumina particles were functionalized with 10 wt. % PEI for 3 h, 6 h, and 9 h. Functionalization did not significantly change the particle size. In contrast, at the end of 3 hours of reaction, the zeta potential increased from 32.14 mV to 44.38 mV. In 6h, the particles' charge reached their peak value of 49.53 mV and decreased to 44.92 mV at 9 h reaction time (Figure 4.8). The optimal reaction time of 6 hours was selected based on the results, as it resulted in the highest zeta potential.

Figure 4.9 illustrates the impact of PEI concentration on the particle size and zeta potential of the modified alumina particles. Within the range of 10 to 20 wt. %, variations in PEI concentration led to comparable zeta potentials and particle sizes. Subsequently, the optimal PEI concentration was determined to be 10 wt.% to minimize PEI consumption.
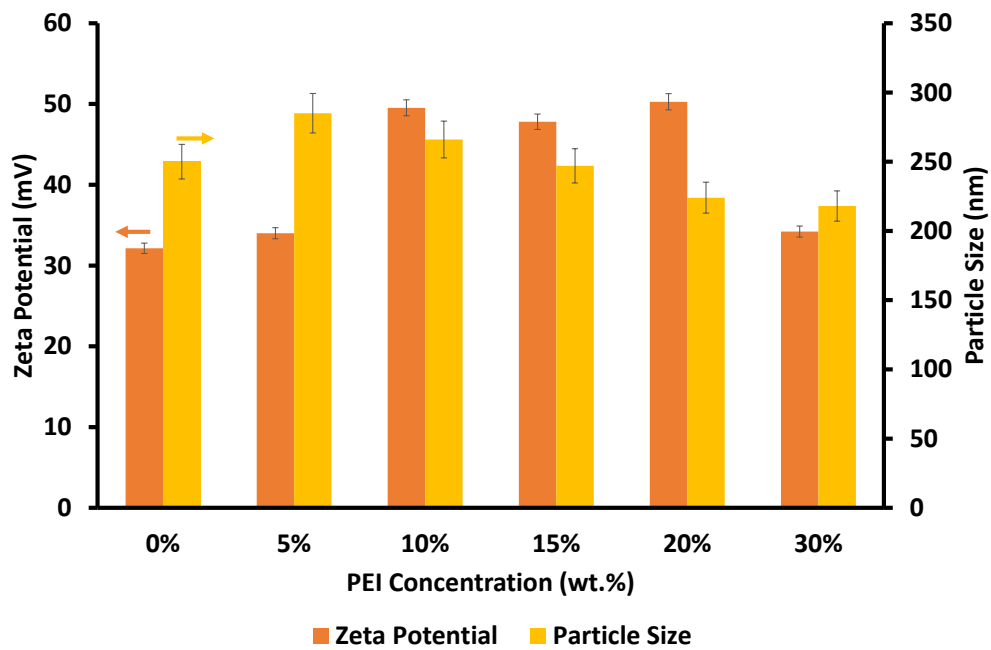
Figure 4.9. The effect of PEI concentration on the particle size and zeta potential of the PEI coated Al_2O_3 particles. Coating time: 6 h.

0.01 wt. % aqueous alumina solution was prepared with the optimum conditions and sonicated for 10 min to prevent agglomeration. Figure 4.10 shows SEM and EDX images of the Al/PDA/PEI-PAI membranes. The elemental composition determined from EDX mapping proved successful immobilization of alumina particles since Al was detected only in the Al/PDA/PEI-PAI membrane (Table 4.2). Additionally, the O_2 amount increased from 23.51% to 28.29% after modification of the PDA/PEI-PAI membrane.
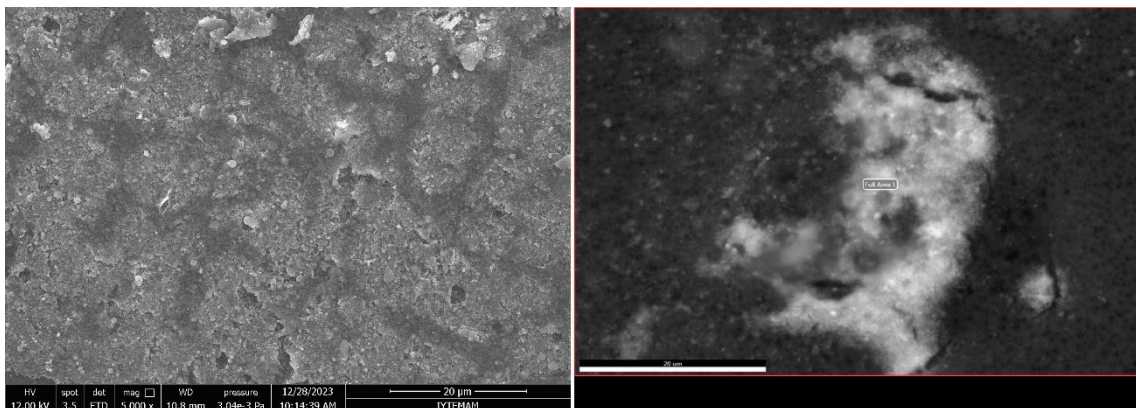
Figure 4.10. SEM and EDX images of the Al/PDA/PEI-PAI membrane

Table 4.2. Elemental analysis of the PDA/PEI-PAI and Al/PDA/PEI-PAI membranes.

Element	PDA/PEI-PAI (wt.%)	Al/PDA/PEI-PAI (wt.%)
C	55.72	54.52
N	20.76	12.88
O	23.51	28.29
Al	0	4.32
Total:	100.00	100.00

Figure 4.11 displays how the membranes' pure water permeability and Mg^{2+} rejection changed with the volume of alumina solution filtered through the membrane at 2.5 bar. Following filtration, the membranes were backwashed with DI water at 2.5 bar to remove the loosely bound particles. As expected, the alumina particle immobilization reduced the PWP, the largest reduction was observed after 26.2 L/m^2 alumina filtration. The optimal filtration time for the alumina solution was determined to be 26.2 L/m^2, as it yielded the highest Mg^{2+} rejection value.
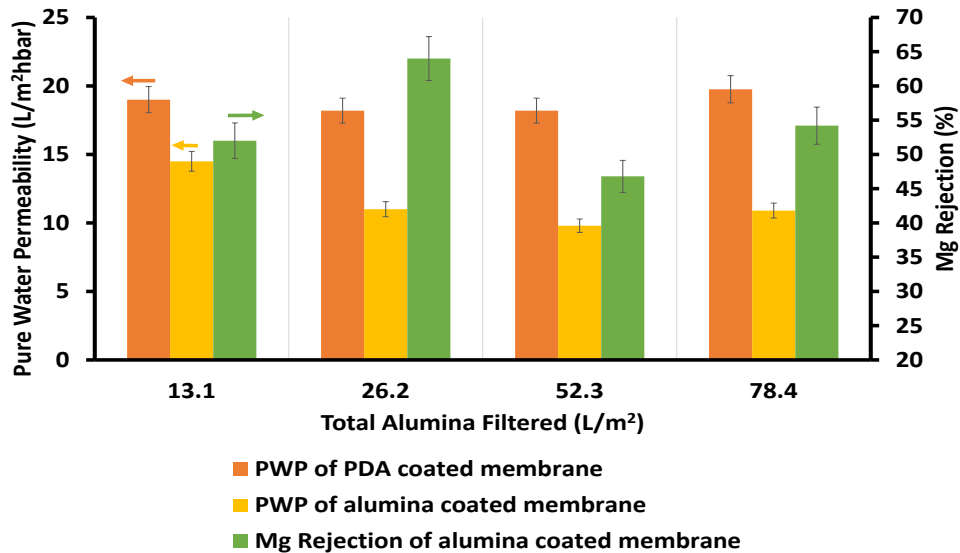
Figure 4.11. The change of pure water permeability and Mg^{2+} rejection as a function of volume of alumina filtered through the membrane. Mg^{2+} concentration: 2000 ppm and transmembrane pressure: 2.5 bar.

4.1.4. Preparation of PEI Coated Al/PDA/PEI/PAI Membranes (PEI/Al/PDA/PEI-PAI)

The Mg^{2+} rejection level should be above 80 % to obtain desired Li^+/Mg^{2+} ratio for Li^+ precipitation process. Thus, in the last step of the membrane preparation, 20 mg/mL PEI (800 Da) aqueous solution was filtered through the Al/PDA/PEI-PAI membrane at 2.5 bar. Following filtration, the membranes were backwashed with ultra-pure water to remove unbounded PEI.

Figure 4.12 shows the SEM and EDX analysis of the PEI-coated Al/PDA/PEI-PAI membrane. Alumina particles are mostly homogeneously distributed on the surface without significant agglomeration. Elemental analysis (Table 4.3) revealed a decrease in oxygen content from 28.29% to 23.26% and an increase in nitrogen content from 12.88% to 16.17% following PEI coating. This transformation is attributed to the interaction between the amine groups in PEI and the quinone structures of oxidized dopamine, forming covalent bonds. The decrease is proof of successful PEI coating on the PDA surface not covered by the alumina particles.
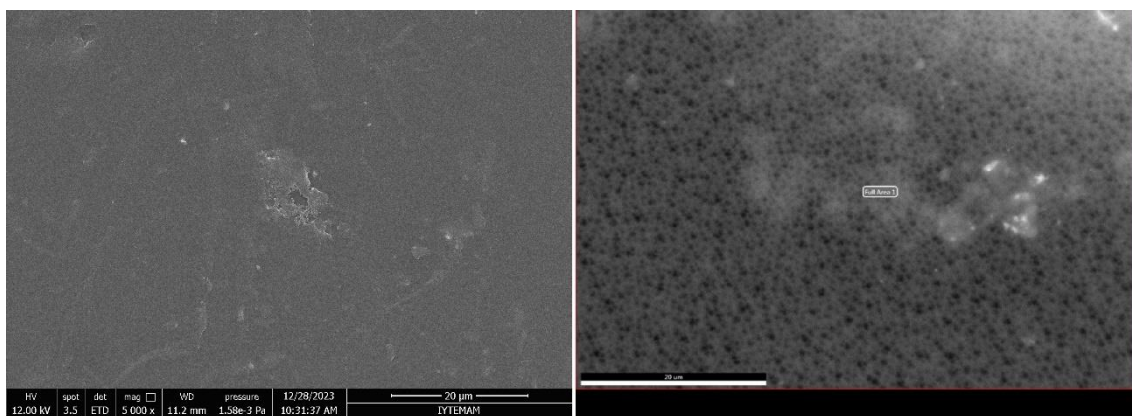
Figure 4.12. SEM and EDX images of the PEI coated Al/PDA/PEI-PAI membrane

Table 4.3. Elemental analysis of the Al/PDA/PEI-PAI and PEI coated Al/PDA/PEI-PAI
membranes.

Element	Al/PDA/PEI-PAI (wt.%)	PEI/Al/PDA/PEI-PAI (wt.%)
C	54.52	58.49
N	12.88	16.17
O	28.29	23.26
Al	4.32	2.08
Total:	100.00	100.00

The AFM images of the Al/PDA/PEI-PAI and PEI-coated Al/PDA/PEI-PAI
membranes are displayed in Figure 4.13. PEI coating reduced the surface roughness from
17 to 11.5 nm, suggesting that the valleys between alumina particles are filled with PEI.
In contrast to the polyamide-based thin film composite membranes, the roughness of the
final membrane is slightly higher than the roughness of the uncovered support.
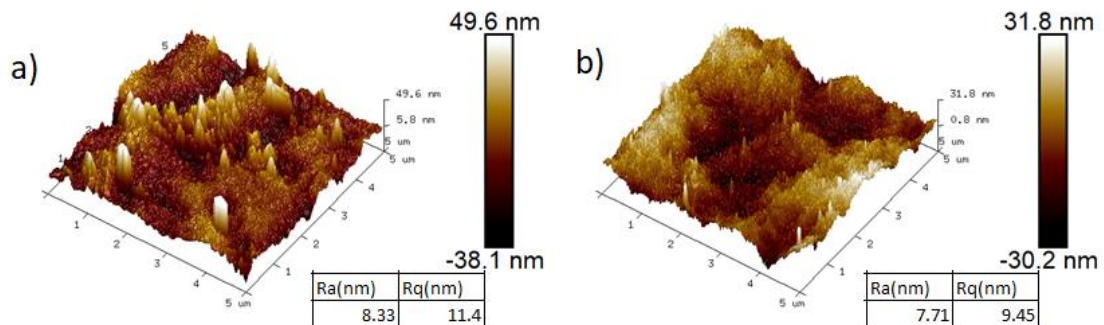
Figure 4.13. AFM images of a) the Al/PDA/PEI-PAI and b) PEI coated Al/PDA/PEI-PAI
membranes

Figure 4.14 illustrates the changes in contact angles after adding each layer on the
support. PDA coating slightly improved the hydrophilicity of the support. However, water
contact angle increased from 77.42±1.33° to 79.09±0.89° after PEI-functionalized
alumina was filtered through the PDA modified support membrane. PDA can easily be
synthesized through the oxidative polymerization of dopamine's catechol groups. The

resulting PDA polymer contains hydroxyl groups at the chain ends. Due to the susceptibility of these terminal hydroxyl groups to oxidation, their interaction with pure oxygen during polymerization leads to oxidation reactions, resulting in the transformation of C-OH bonds in the structure into C=O bonds[58]. The presence of C=O groups in the PDA structure and the presence of NH_2 groups in PEI-functionalized alumina led to the occurrence of a Schiff base reaction, resulting in the breaking of the C=O bond and the formation of C=N groups[59]. The electronegativity difference for C=N (0.49) is lower than that for C=O (0.89), indicating a weaker polarization in C=N. As a result, C=N is expected to contribute to a less hydrophilic surface compared to C=O. The filtration of PEI in the last step of membrane preparation resulted in a further increase in the contact angle from 79.09±0.89° to 85.55±0.98°. This increase occurs because PEI continues to substitute free C=O groups in the PDA structure with C=N groups, resulting in a decrease in the membrane's hydrophilicity.
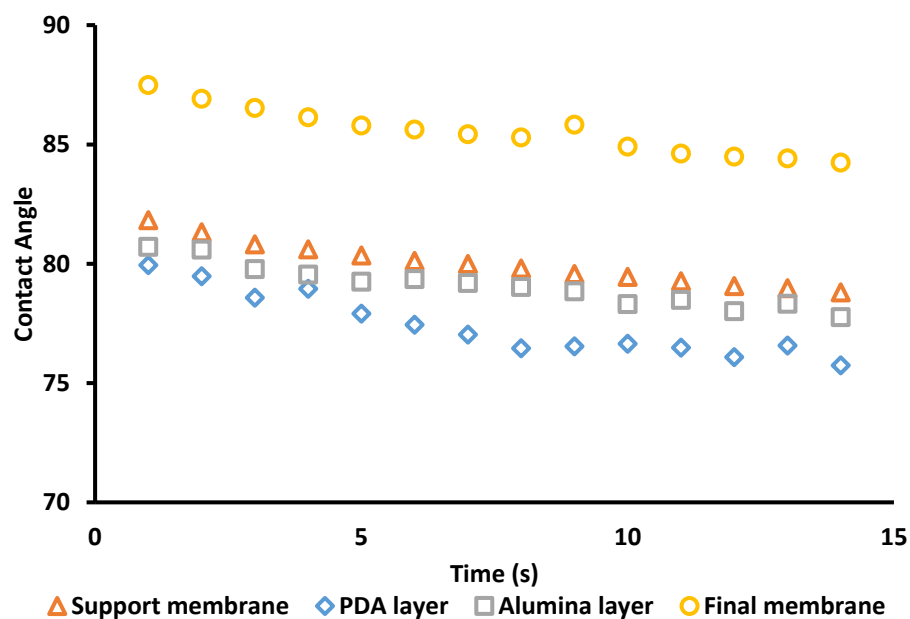
Figure 4.14. The change of contact angle value of the support membrane upon adding each layer on top of it.

The main objective of this thesis is to achieve high Li^+ purity and high Li^+ recovery. Thus, the final membrane performance was evaluated by measuring the pure water permeability, Mg^{2+}, and Li^+ rejections of the salt mixture with a Mg^{2+}: Li^+ ratio of

20:1 wt.%. The following performance criterion was proposed to consider the effects of Li^+, Mg^{2+} and water permeability.

$$PP = Li_{Purity} \times Li_{Recovery} = {P_{Li}}/{P_{Mg}} \times {P_{Li}}/{P_{Water}} \qquad (4.1)$$

where, $P_{Li,}$ P_{Mg}, P_{water} are the permeabilities of Li^+, Mg^{2+} and water through the membrane, respectively.
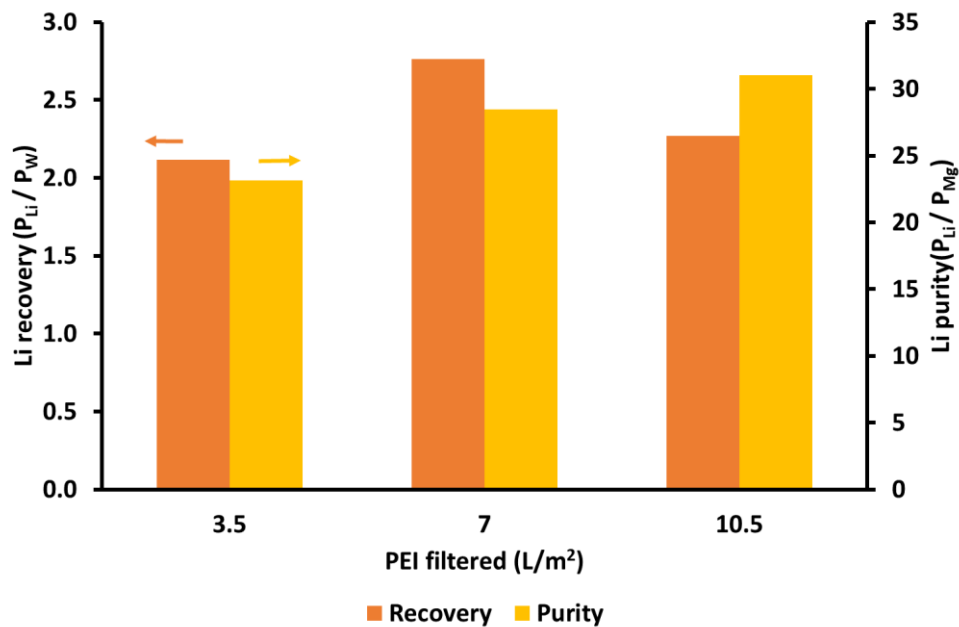
Figure 4.15. The change of performance parameter of the PEI coated Al/PDA/PEI-PAI membranes as a function of volume of PEI filtered through the membrane.

Equation 4.1 implies that to achieve a high-performance parameter, it is desirable for the water and Mg2+ permeability of the membrane to be as low as possible, while the Li+ permeability should be as high as possible. 800 Da PEI was filtered through the Al/PDA/PEI-PAI membrane at three different volumes. The results in Figure 4.15 show that 7 L/m² PEI filtration resulted in the highest performance parameter and, thus, was chosen as the optimum value.

41

4.2. Performance Tests of the Membranes

According to the steric, electric, and dielectric exclusion model (DSPM) (2.1), transport of ions through a NF membrane is controlled by a combination of size exclusion, Donnan exclusion and dielectric exclusion. To demonstrate the contribution of size exclusion, first, the average pore size of the membrane was predicted by determining its molecular weight cutoff value from the retention of neutral sugar molecules. Table 4.4 lists the solutes used in retention tests and their Stokes radius values.

Table 4.4. Molecular weights and stokes radii of neutral molecules.

Solute	Glucose	Sucrose	PEG 400	PEG 600
MW (Da)	180.16	342.3	400	600
r_s (nm)	0.369	0.486	0.520	0.618

The variation in solute retention as a function of the molecular weight is depicted in Figure 4.16. Furthermore, Figure 4.17 illustrates the pore size distribution of the membrane. According to the data presented in Figure 4.16 and Figure 4.17, the molecular weight cutoff of the membrane was identified as 379 Da, and the average pore size was determined to be 0.378 nm.
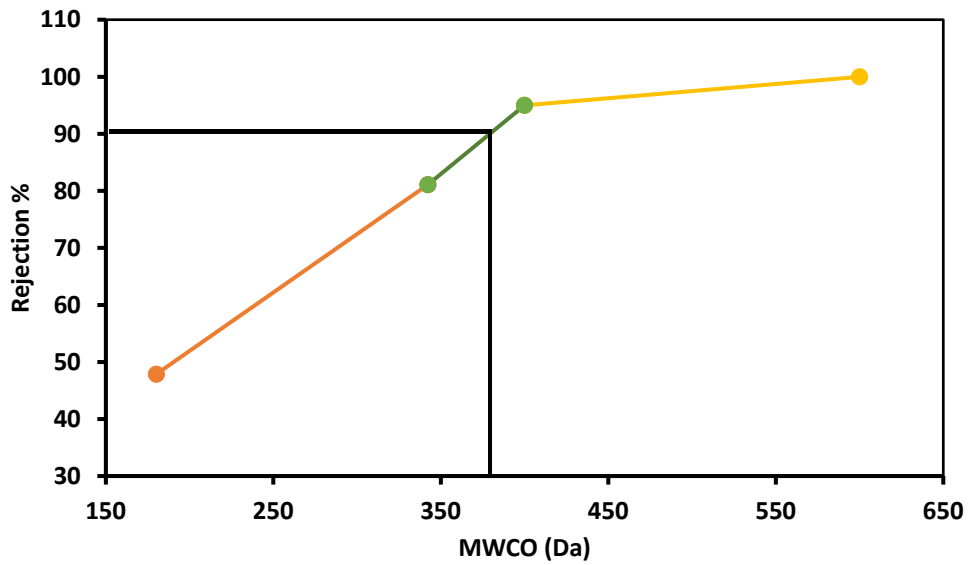
Figure 4.16. Retention rate of neutral solutes by the PEI coated Al/PDA/PEI-PAI membrane.
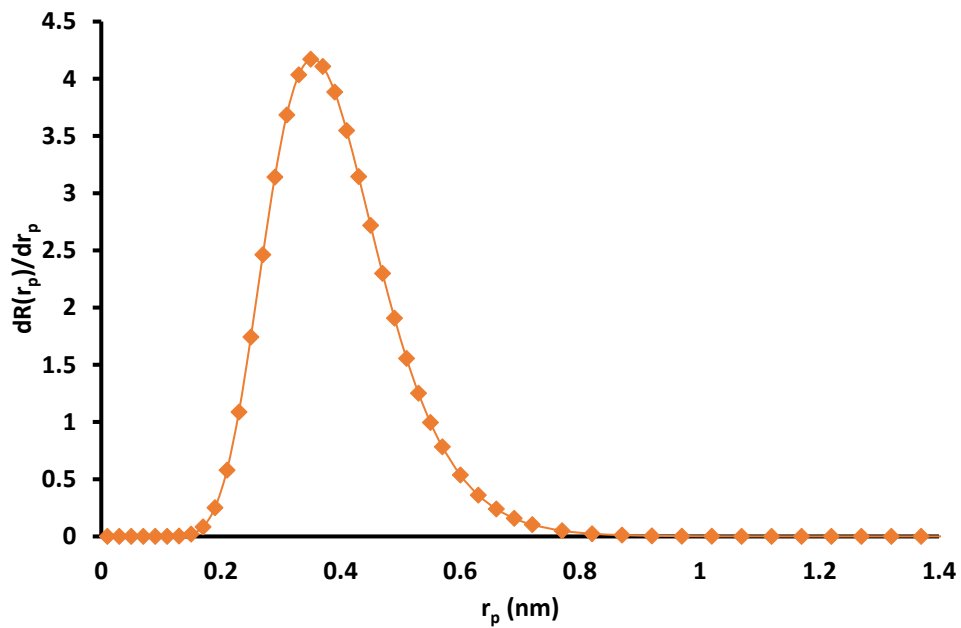
Figure 4.17. The pore size distribution of the PEI coated Al/PDA/PEI-PAI membrane.

The PEI coated Al/PDA/PEI-PAI membrane retained 89% of Mg^{2+} while allowing the passage of the Li^+ in the feed stream, resulting in a -21% rejection. Based on the pore size distribution, it is evident that there are pores larger than the hydrated radius of Mg^{2+}. This observation suggests that high Mg^{2+} rejection cannot be solely explained by size

exclusion alone. To evaluate the contribution of Donnan exclusion that is mainly controlled by the surface charge of the membrane, the zeta potential of the membrane at 6.4 pH corresponding to the pH of the 2000 ppm Li^+ and Mg^{2+} salt solution (Mg^{2+}: Li^+ ratio: 20 wt.%) was measured. Figure 4.18 displays how the zeta potential changed after adding each layer of the final membrane.
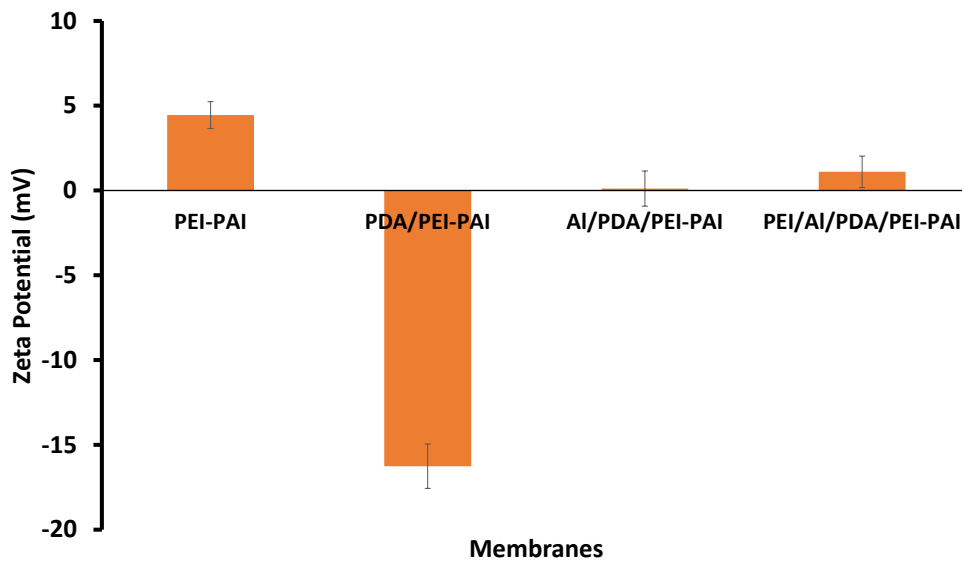
Figure 4.18. Zeta potential of each layer of the membrane at pH 6.7.

The support membrane has a positive zeta potential value due to presence of amine groups in the polyethyleneimine structure. On the other hand, coating with dopamine switched the zeta potential to a negative value resulting from the deprotonation of phenolic hydroxyl groups[60,61]. After alumina particle immobilization, the membrane surface becomes neutral indicating that the amine groups in the PEI structure completely crosslinked with PDA through Michael addition and Schiff base reaction[62]. Finally, the PEI coating at the last stage of membrane preparation slightly increased the surface charge. However, the positive charge of the PEI coated Al/PDA/PEI-PAI membrane is not enough to provide a significant Donnan exclusion for the Mg^{2+} ions. As indicated by Equation 2.1, the ionic valence of Mg^{2+} enhances its rejection by the dielectric exclusion, with rejection being proportional to the square of the ionic valence. Besides, Yaroshchuk showed that [47] dielectric exclusion effects are strong for neutral NF membranes since the

fixed charges on the pore walls weakens dielectric exclusion effects by screening the image charge forces. Consequently, an increase in fixed charge density within the NF membrane enhances Donnan exclusion, but concurrently screens and diminishes the strength of DE[63].

The PEI/Al/PDA/PEI-PAI membrane is relatively hydrophobic (contact angle is 85.55±0.98°) and hydrophobicity enhances the effect of the dielectric exclusion. The hydration energy of Mg^{2+} (-1828 kJ/mol) is much higher than that of Li^+ (-515 kJ/mol). Thus, the hydrophobic domains in the membrane hinder the permeation of strongly hydrated Mg^{2+} and allows the passage of less hydrated Li^+ [64].

These observations then clearly demonstrate that the PEI coated Al/PDA/PEI-PAI membrane controls the separation of Mg^{2+} from Li^+ by a combination of size and dielectric exclusion.

4.3 Performance Test of the PEI/Al/PDA/PEI-PAI Membrane

Table 4.5 show that most previous studies evaluate membrane performance in a plot of Li^+/Mg^{2+} selectivity vs. water permeability. In these studies, the main aim is to develop membranes with both high permeability and high selectivity; however, these criteria are suitable when water recovery is the primary objective of the separation. An ideal NF membrane for Li^+/Mg^{2+} separation should produce Li^+ with desired purity by allowing fast Li^+ permeation and slow Mg^{2+} permeation. High water permeability can reduce energy consumption and area requirement, thus, reducing the cost of separation. However, water permeation should not exceed the Li^+ permeation rate to achieve a high Li^+ purity. Based on these considerations, Wang et al.[10] proposed two new performance criteria. The first is the Li^+ permeability over the Mg^{2+} permeability (P_{Li}/P_{Mg}) rate through the membrane, and the second one is the Li^+ permeability over water permeability (P_{Li}/P_w) rate. An ideal NF membrane should have high P_{Li}/P_{Mg} to achieve a product with high Li^+ purity and high P_{Li}/P_w ratio to have a Li^+ recovery rate. The primary purpose of integrating membrane separation into the Li^+ purification process is to increase the feasibility of the process. NF membranes can decrease Mg^{2+} subordinates in feed solutions, increase Li^+ content, and increase profitability.

Table 4.5. MWCO, salt rejection and Pi/P$_w$ and P$_{Li}$/P$_{Mg}$ ratios reported by different studies in literature.

MWCO (Da)	Li$^+$ Rejection	Mg^{2+} Rejection	P$_{Li}$/P$_w$ (bar) [10]	P$_{Li}$/P$_{Mg}$ [10]	S$_{Li/Mg}$	Refs.
285	18	95	2.2	26.4	NA	[15]
340	19	95	3.8	26.6	20	[13]
704	20.9	95.1	0.9	25.9	16.1	[32]
310	5.2	97.2	1.7	54.1	33.4	[29]
278	NA	NA	2.1	15.0	12.7	[65]
734	21.76	96.11	3.7	31.7	12.15	[14]
734	11.6	95.6	3.3	31.7	5.84	[14]
NA	NA	NA	NA	NA	5.2	[31]
1000	32.3	91.6	1.9	12.8	8	[34]
490	NA	NA	8.0	20.0	8.12	[66]
NA	11.5	98.5	NA	NA	58.66	[33]
226	NA	98.0	NA	NA	50.7	[67]
248	NA	NA	NA	NA	9.22	[16]
859	14.9	97.1	NA	NA	28	[18]

(cont. on next page)

Table 4.5 (cont.)

646	NA	NA	NA	NA	10.1	[30]
291	35.2	99.1	NA	NA	35.7	[27]
NA	31.5	91.7	NA	NA	11.9	[54]
200-250	NA	95	NA	NA	13	[23]
200-400	15	96	NA	NA	42	[63]
150-200	5.34	86.7	NA	NA	7.15	[20]
430	NA	97.4	0.9	38.0	23.9	[25]

NA: Not Available

Table 4.6. Filtration conditions reported by different studies in literature.

Filtration System	Concentration	Mg^{2+}/Li$^+$ Ratio	Pressure (bar)	Refs.
Cross-flow filtration unit	2000 ppm	Mass Ratio: 21.4	4	[15]
Cross-flow filtration unit	2000 ppm	Mass Ratio: 20.0	8	[13]
Cross-flow filtration unit	2000 ppm	Mass Ratio: 20.0	3	[32]
Cross-flow filtration unit	2000 ppm	Mass Ratio: 20.0	4	[29]
Cross-flow filtration unit	2.4 g/L Mg^{2+}	Mass Ratio: 24.0	10	[65]
Cross-flow filtration unit	2000 ppm	Mass Ratio: 30.0	8	[14]
Cross-flow filtration unit	2000 ppm	Mass Ratio: 60.0	8	[14]
Cross-flow filtration unit	2000 ppm	Mass Ratio: 50.0	6	[31]
Cross-flow filtration unit	2000 ppm	Mass Ratio: 23.0	5	[34]
Dead-end filtration unit	2000 ppm	Mass Ratio: 20.0	6	[66]
Cross-flow filtration unit	2000 ppm	Mass Ratio: 20.0	3	[33]
Cross-flow filtration unit	2000 ppm	Mass Ratio: 27.3	10	[67]
Cross-flow filtration unit	2000 ppm	Mass Ratio: 20.0	15	[16]

Table 4.6 (cont.)

Cross-flow filtration unit	MgCl$_2$:2000 ppm, LiCl: 100 ppm	Mass Ratio: 20.0	6	[18]
Cross-flow filtration unit	2000 ppm	Mass Ratio: 50.0	6	[30]
Cross-flow filtration unit	2000 ppm	Mass Ratio: 21.4	10	[27]
Cross-flow filtration unit	2000 ppm	Mass Ratio: 20.0	5	[54]
Cross-flow filtration unit	MgCl$_2$.6H$_2$O 58, LiCl:1.25 g/L	Mass Ratio: 35	changing	[23]
Spiral wound	6000ppm	Mole Ratio: 40	6	[63]
Dead-end unit	C$_{Li}$:0.392, C$_{Mg}$:11.59 g/L	Mole Ratio: 30	NA	[20]
Cross-flow filtration unit	2000ppm	Mass Ratio: 73	4	[25]

NA: Not Available

Table 4.7. Pure water permeability, salt rejection and permeability rates of reported membranes on the literature (The table exclusively includes data for the separation of a 2000 ppm salt mixture with a Li$^+$: Mg^{2+} ratio of 1:20, conducted at transmembrane pressures of 3-6 bar.)

Pure Water Flux (L/m^{2}h)	Pressure (bar)	Mg Rejection (%)	Li Rejection (%)	P$_{Li}$/P$_w$ (bar)	P$_{Li}$/P$_{Mg}$	Ref.
36.0	3	95.1	20.9	0.9	25.9	[32]
48.0	4	97.2	5.0	2.0	58.9	[29]
34.5	3	98.5	11.5	0.8	90.9	[33]
72.0	6	97.1	14.9	3.7	31.7	[18]
50.0	5	91.7	31.5	2.1	11.9	[54]
56.0	4	95.0	18.0	2.2	26.4	[15]
81.0	5	92.0	33.0	1.9	12.8	[35]
34.0	3.5	89.0	-21.0	3.6	106.9	This work

Figure 4.19 shows the tradeoff between Li^+ purity and Li^+ recovery. Pure water permeability was calculated from the pure water flux measured at the set value of transmembrane pressure. Li^+ and Mg^{2+} permeabilities were estimated from the solution-diffusion-electromigration (SDEM) model[10]. It should be emphasized that ion permeabilities depend on feed composition; thus, only the data collected with 2000 ppm salt mixture containing 1:20 Li^+: Mg^{2+} ratio was used for comparison. The transmembrane pressure value used for collecting the data in Table 4.5 varied between 3-6 bars. The raw data used in Figure 4.19 are listed in Table 4.7.
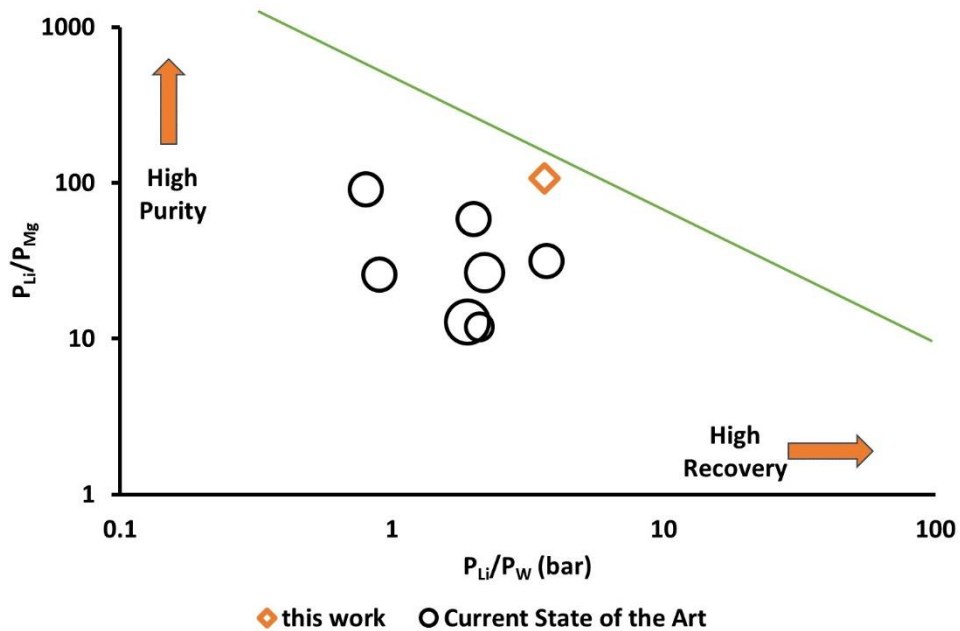
Figure 4.19. The plot of P_{Li}/P_{Mg} versus P_{Li}/P_w in comparison with those of recently reported membranes. The line in represents the Li^+ purity-recovery trade-off for the current membranes.

Both high Li^+ purity and high Li^+ recovery are the desirable features for the membrane. Upon examining the data, it becomes apparent that both the Mg^{2+} and Li^+ rejections reported in previous studies are greater than the findings presented in this thesis. High Li^+ rejections of around 30 % caused low Li^+ purities. A membrane demonstrating high Li^+ rejection can contribute to achieving elevated Li^+ purity, particularly in cases where Mg^{2+} rejection reaches significant levels. High water permeabilities are desirable, provided that they do not surpass the permeability of Li^+.

The P_{Li}/P_w ratio corresponds to Li^+ recovery; therefore, this ratio should exceed 1. According to the data in Table 4.5 the membrane prepared in this thesis demonstrated the highest Li^+ recovery and purity. The second-highest Li^+ purity (P_{Li}/P_{Mg}:91) was reported by Xu et al.[33] for the TFC membrane, which was prepared through interfacial polymerization on the PES support modified with potassium carboxylate functionalized multi-walled carbon nanotubes. However, this membrane cannot provide high Li^+ recovery, as evidenced by the P_{Li}/P_w ratio being less than 1. On the other hand, Wu et al.[18] reported an equivalent Li^+ recovery value to that obtained in this study by applying a transmembrane pressure that was 2 times higher; however, the Li^+ purity achieved with their membrane was considerably lower. It can be concluded that under conditions of 2000 ppm salt concentration and a Li^+: Mg^{2+} ratio of 1:20, the membrane developed in this thesis exhibited the highest Li^+ purity and Li^+ recovery compared to membranes reported in the literature tested under the same conditions.

4.4 Long-Term Stability of the PEI/Al/PDA/PEI-PAI Membrane

The long-term stability of the PEI/Al/PDA/PEI-PAI membrane was tested under static and dynamic conditions. Figure 4.20 displays how the pure water permeability, Li^+ rejection, and Mg^{2+} rejection changed over time after storing the membrane in a 2000 ppm Li^+:Mg^{2+} salt mixture (1:20 mass ratio) for up to 30 days. The data collected during the first week of testing exhibited slight fluctuations; however, after 7 days, both the pure water permeability and ion rejections showed no significant changes over time.
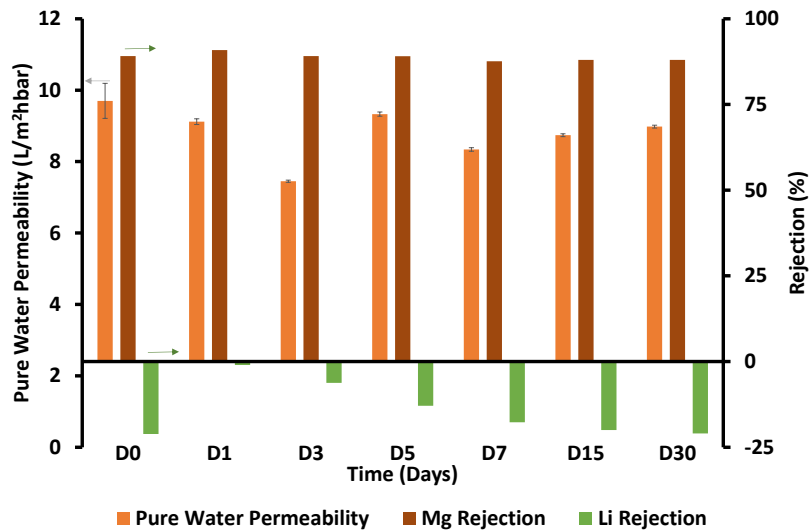
Figure 4.20. The change of pure water permeability, Li$^+$ and Mg^{2+} rejections after storing the membrane in a 2000 ppm Li$^+$: Mg^{2+} salt mixture (1:20 mass ratio).

The overall long-term performance of the membrane is better assessed by examining the variation of the separation factor. Figure 4.21 illustrates that the separation factor of the membrane remained constant at 10 during one month of storage in the salt solution.
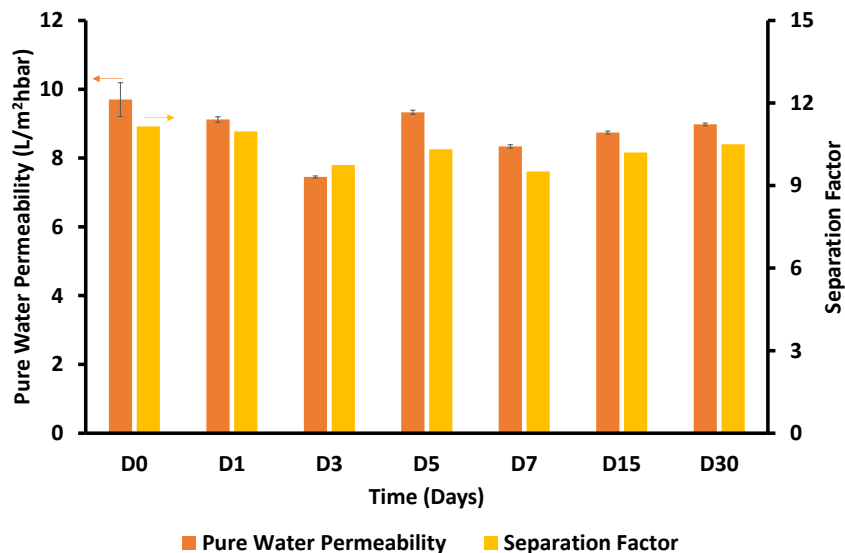
Figure 4.21. The change of separation factor with time after storing the membrane in a 2000 ppm Li$^+$: Mg^{2+} salt mixture (1:20 mass ratio).

The results of the aluminum nanoparticle release test revealed that 11.85 g/m^2 of aluminum atoms were impregnated on the membrane surface. A membrane sample of 28.7 cm^2 was stored in a 50 mL salt mixture and analyzed using ICP-MS. The test results indicated that the aluminum concentration in samples stored for 1, 3, 5, 7, 15, and 30 days was below the detection limit of 5 ppb. Therefore, these findings indicate the stability of the impregnated alumina within the membrane structure.

The Li$^+$ and Mg^{2+} rejections also remained constant during the 72-hour dynamic filtration test. The results implicitly demonstrate the stability of the alumina particles, PDA, and PEI layers on the support membrane, as evidenced by the significantly different Mg^{2+} rejection values for the Al/PDA/PEI-PAI and the PEI/Al/PDA/PEI-PAI membranes (Figure 4.22). Additionally, the salt flux did not change during the 72-hour filtration, providing evidence of the membrane's antifouling property. The PEI/Al/PDA/PEI-PAI membrane is relatively hydrophobic as indicated by the contact angle value close to 90° (Figure 4.14). Thus, the antifouling property of this membrane can be attributed to the relatively smooth nearly neutral surface acting like a zwitterionic surface.
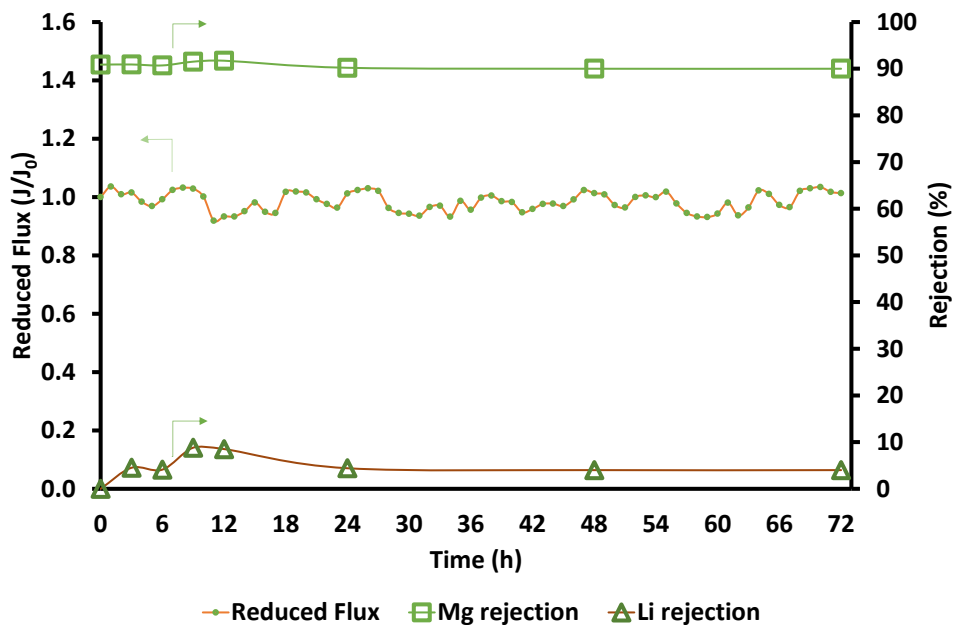
Figure 4.22. The change of pure water permeability, Li$^+$ and Mg^{2+} rejections during filtration of 2000 ppm Li$^+$: Mg^{2+} salt mixture (1:20 mass ratio).

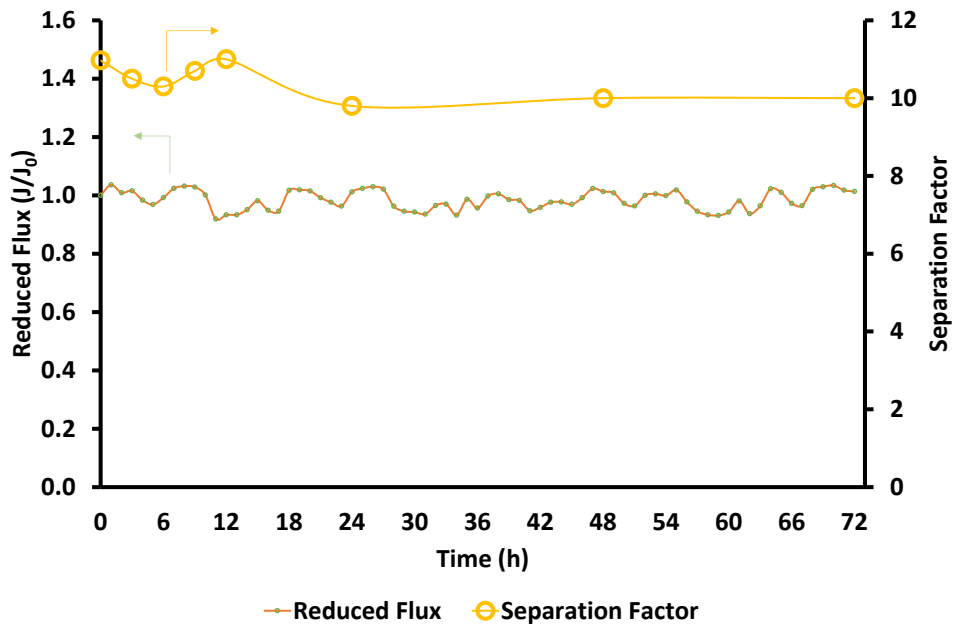Figure 4.23. The change of pure water permeability and separation factor during filtration of 2000 ppm Li^+: Mg^{2+} salt mixture (1:20 mass ratio).

CHAPTER 5

CONCLUSIONS

In this thesis, a novel NF membrane was developed for an efficient Li^+-Mg^{2+} separation. The support membrane was prepared using the nonsolvent-induced phase inversion technique and optimized by adjusting the PAI content, casting thickness, and the solvent: cosolvent ratio. The optimization was guided by finding a balance between pure water permeability and rejection of PEG (6 kDa and 1 kDa). Two parameters were identified as effective in reducing the pore size of the support: 1) Incorporating a co-solvent into the casting solution, and 2) Introducing a high molecular weight PEI (25 kDa) into the coagulation bath. The optimum support preparation conditions were found as follows: 17% PAI content, a 1:5 Dioxane: NMP ratio, a casting thickness of 200 μm, and a coagulation medium of water containing 5 g/L PEI. The in situ-generated polydopamine layer on the support membrane served as a bridge for subsequent layer deposition. A coating time of 20 minutes yielded the highest rejection for PEG 1 kDa and the least reduction in pure water permeability. The quantity of alumina particles filtered through the membrane was optimized with a focus on achieving the highest Mg^{2+} rejection rate. Simultaneously, the amount of filtered PEI was adjusted considering both Li^+ and Mg^{2+} rejections.

Membrane production method and number of layers in the selective layer were limited to facilitate scalability. Produced membranes can be easily scaled up for large scale applications because the used materials do not require post and pre-treatment applications and they are relatively cheaper than materials like MWCNTs. Support membrane was produced by the most used membrane production method, phase inversion, and selective layer modified by single 3-layer.

The nanofiltration (NF) membrane, produced under individually optimized conditions for each layer, exhibited a rejection rate of approximately 90% for Mg^{2+} and around -21% for Li^+, while maintaining a pure water permeability of 9.7 L/m²hbar. The membrane features a surface that is relatively hydrophobic and nearly neutral, facilitating the separation of Li^+/Mg^{2+} through a combination of steric hindrance and dielectric exclusion. The membrane performance, evaluated in terms of salt flux, Li^+ and Mg^{2+}

rejections, demonstrated stability even after being stored in a 2000 ppm simulated brine solution containing Li^+ and Mg^{2+} at a ratio of 1:20 for up to 30 days. Likewise, a 72-hour dynamic filtration of simulated brine affirmed the stability of the membrane performance. This study demonstrated that relatively hydrophobic and neutral NF membranes hold promise for efficiently separating Li^+/Mg^{2+}. The membrane developed in this thesis demonstrated the highest levels of Li^+ purity and Li^+ recovery when compared to membranes documented in the literature and tested under identical conditions as those employed in this study.

REFERENCES

(1)   Xu, P.; Hong, J.; Qian, X.; Xu, Z.; Xia, H.; Tao, X.; Xu, Z.; Ni, Q. Q. Materials for Lithium Recovery from Salt Lake Brine. *Journal of Materials Science*. Springer January 1, **2021**, pp 16–63. https://doi.org/10.1007/s10853-020-05019-1.

(2)   Geological Survey, U. *Mineral Commodity Summaries* **2022**.

(3)   National Minerals Information Center, U. *Mcs2020.Pdf - Mineral Commodity Summaries* **2020**.

(4)   Li, X.; Mo, Y.; Qing, W.; Shao, S.; Tang, C. Y.; Li, J. Membrane-Based Technologies for Lithium Recovery from Water Lithium Resources: A Review. *Journal of Membrane Science*. Elsevier B.V. December 1, **2019**. https://doi.org/10.1016/j.memsci.2019.117317.

(5)   Zhang, T.; Zheng, W.; Wang, Q.; Wu, Z.; Wang, Z. Designed Strategies of Nanofiltration Technology for Mg^{2+}/Li^+ Separation from Salt-Lake Brine: A Comprehensive Review. *Desalination*. Elsevier B.V. January 15, **2023**. https://doi.org/10.1016/j.desal.2022.116205.

(6)   Zhu, R.; Wang, S.; Srinivasakannan, C.; Li, S.; Yin, S.; Zhang, L.; Jiang, X.; Zhou, G.; Zhang, N. Lithium Extraction from Salt Lake Brines with High Magnesium/Lithium Ratio: A Review. *Environmental Chemistry Letters*. Springer Science and Business Media Deutschland GmbH June 1, **2023**. https://doi.org/10.1007/s10311-023-01571-9.

(7)   Schmidt, A.; Mestmäcker, F.; Brückner, L.; Elwert, T.; Strube, J. Liquid-Liquid Extraction and Chromatography Process Routes for the Purification of Lithium. In *Materials Science Forum*; Trans Tech Publications Ltd, **2019**; Vol. 959 MSF, pp 79–99. https://doi.org/10.4028/www.scientific.net/MSF.959.79.

(8)   Garcia, L. V.; Ho, Y. C.; Myo Thant, M. M.; Han, D. S.; Lim, J. W. Lithium in a Sustainable Circular Economy: A Comprehensive Review. *Processes*. MDPI February 1, **2023**. https://doi.org/10.3390/pr11020418.

(9)   Zhang, Y.; Wang, L.; Sun, W.; Hu, Y.; Tang, H. Membrane Technologies for Li^+/Mg^{2+} Separation from Salt-Lake Brines and Seawater: A Comprehensive

Review. *Journal of Industrial and Engineering Chemistry* **2020**, *81*, 7–23. https://doi.org/10.1016/J.JIEC.2019.09.002.

(10) Wang, R.; Lin, S. Performance Metrics for Nanoltration-Based Selective Separation for Resource Extraction and Recovery. **2022**. https://doi.org/10.21203/rs.3.rs-1972307/v1.

(11) Hoek, E. M.; Pendergast, M. M. *Encyclopedia of Membrane Science and Technology, John Wiley & Sons Canada, Limited, Hoboken, NJ*; **2013**.

(12) Jye, L. W.; Ismail, A. F. *Nanofiltration Membranes*; CRC Press, **2016**. https://doi.org/10.1201/9781315181479.

(13) Xu, P.; Wang, W.; Qian, X.; Wang, H.; Guo, C.; Li, N.; Xu, Z.; Teng, K.; Wang, Z. Positive Charged PEI-TMC Composite Nanofiltration Membrane for Separation of Li^+ and Mg^{2+} from Brine with High Mg^{2+}/Li^+ Ratio. *Desalination* **2019**, *449*, 57–68. https://doi.org/10.1016/j.desal.2018.10.019.

(14) Guo, C.; Li, N.; Qian, X.; Shi, J.; Jing, M.; Teng, K.; Xu, Z. Ultra-Thin Double Janus Nanofiltration Membrane for Separation of Li^+ and Mg^{2+}: "Drag" Effect from Carboxyl-Containing Negative Interlayer. *Sep Purif Technol* **2020**, *230*. https://doi.org/10.1016/j.seppur.2019.05.009.

(15) Zhang, H. Z.; Xu, Z. L.; Ding, H.; Tang, Y. J. Positively Charged Capillary Nanofiltration Membrane with High Rejection for Mg^{2+} and Ca^{2+} and Good Separation for Mg^{2+} and Li^+. *Desalination* **2017**, *420*, 158–166. https://doi.org/10.1016/j.desal.2017.07.011.

(16) Li, Y.; Wang, S.; Wu, W.; Yu, H.; Che, R.; Kang, G.; Cao, Y. Fabrication of Positively Charged Nanofiltration Membrane with Uniform Charge Distribution by Reversed Interfacial Polymerization for Mg^{2+}/Li^+ Separation. *J Memb Sci* **2022**, *659*. https://doi.org/10.1016/j.memsci.2022.120809.

(17) Dobosz, K. M.; Kuo-Leblanc, C. A.; Emrick, T.; Schiffman, J. D. Antifouling Ultrafiltration Membranes with Retained Pore Size by Controlled Deposition of Zwitterionic Polymers and Poly(Ethylene Glycol). *Langmuir* **2019**, *35* (5), 1872–1881. https://doi.org/10.1021/acs.langmuir.8b02184.

(18) Wu, M. B.; Ye, H.; Zhu, Z. Y.; Chen, G. T.; Ma, L. L.; Liu, S. C.; Liu, L.; Yao, J.; Xu, Z. K. Positively-Charged Nanofiltration Membranes Constructed via

Gas/Liquid Interfacial Polymerization for Mg^{2+}/Li^+ Separation. *J Memb Sci* **2022**, *644*. https://doi.org/10.1016/j.memsci.2021.119942.

(19)   Tekinalp, Ö.; Alsoy Altinkaya, S. Development of High Flux Nanofiltration Membranes through Single Bilayer Polyethyleneimine/Alginate Deposition. *J Colloid Interface Sci* **2019**, *537*, 215–227. https://doi.org/10.1016/j.jcis.2018.10.089.

(20)   Ashraf, M. A.; Wang, J.; Wu, B.; Cui, P.; Xu, B.; Li, X. Enhancement in Li^+/Mg^{2+} Separation from Salt Lake Brine with PDA–PEI Composite Nanofiltration Membrane. *J Appl Polym Sci* **2020**, *137* (47). https://doi.org/10.1002/app.49549.

(21)   Yang, G.; Shi, H.; Liu, W.; Xing, W.; Xu, N. Investigation of Mg^{2+}/Li^+ Separation by Nanofiltration. *Chin J Chem Eng* **2011**, *19* (4), 586–591. https://doi.org/10.1016/S1004-9541(11)60026-8.

(22)   Pramanik, B. K.; Asif, M. B.; Kentish, S.; Nghiem, L. D.; Hai, F. I. Lithium Enrichment from a Simulated Salt Lake Brine Using an Integrated Nanofiltration-Membrane Distillation Process. *J Environ Chem Eng* **2019**, *7* (5), 103395. https://doi.org/10.1016/J.JECE.2019.103395.

(23)   Li, Y.; Zhao, Y. J.; Wang, H.; Wang, M. The Application of Nanofiltration Membrane for Recovering Lithium from Salt Lake Brine. *Desalination* **2019**, *468*. https://doi.org/10.1016/j.desal.2019.114081.

(24)   Sun, S. Y.; Cai, L. J.; Nie, X. Y.; Song, X.; Yu, J. G. Separation of Magnesium and Lithium from Brine Using a Desal Nanofiltration Membrane. *Journal of Water Process Engineering* **2015**, *7*, 210–217. https://doi.org/10.1016/J.JWPE.2015.06.012.

(25)   Bi, Q.; Zhang, C.; Liu, J.; Liu, X.; Xu, S. Positively Charged Zwitterion-Carbon Nitride Functionalized Nanofiltration Membranes with Excellent Separation Performance of Mg^{2+}/Li^+ and Good Antifouling Properties. *Sep Purif Technol* **2021**, *257*. https://doi.org/10.1016/j.seppur.2020.117959.

(26)   Aghili, F.; Ghoreyshi, A. A.; Van der Bruggen, B.; Rahimpour, A. A Highly Permeable $UiO-66-NH_2$/Polyethyleneimine Thin-Film Nanocomposite Membrane for Recovery of Valuable Metal Ions from Brackish Water. *Process Safety and Environmental Protection* **2021**, *151*, 244–256. https://doi.org/10.1016/J.PSEP.2021.05.022.

(27)   Hu, P.; Yuan, B.; Niu, Q. J.; Chen, K.; Xu, Z.; Tian, B.; Zhang, X. Modification of Polyamide Nanofiltration Membrane with Ultra-High Multivalent Cations

Rejections and Mono-/Divalent Cation Selectivity. *Desalination* **2022**, *527*. https://doi.org/10.1016/j.desal.2022.115553.

(28) Lu, D.; Ma, T.; Lin, S.; Zhou, Z.; Li, G.; An, Q.; Yao, Z.; Sun, Q.; Sun, Z.; Zhang, L. Constructing a Selective Blocked-Nanolayer on Nanofiltration Membrane via Surface-Charge Inversion for Promoting Li^+ Permselectivity over Mg^{2+}. *J Memb Sci* **2021**, *635*, 119504. https://doi.org/10.1016/J.MEMSCI.2021.119504.

(29) Yang, Z.; Fang, W.; Wang, Z.; Zhang, R.; Zhu, Y.; Jin, J. Dual-Skin Layer Nanofiltration Membranes for Highly Selective Li^+/Mg^{2+} Separation. *J Memb Sci* **2021**, *620*. https://doi.org/10.1016/j.memsci.2020.118862.

(30) Luo, H.; Peng, H.; Zhao, Q. High Flux Mg^{2+}/Li^+ Nanofiltration Membranes Prepared by Surface Modification of Polyethylenimine Thin Film Composite Membranes. *Appl Surf Sci* **2022**, *579*. https://doi.org/10.1016/j.apsusc.2021.152161.

(31) Feng, Y.; Peng, H.; Zhao, Q. Fabrication of High Performance Mg^{2+}/Li^+ Nanofiltration Membranes by Surface Grafting of Quaternized Bipyridine. *Sep Purif Technol* **2022**, *280*, 119848. https://doi.org/10.1016/J.SEPPUR.2021.119848.

(32) Xu, P.; Hong, J.; Qian, X.; Xu, Z.; Xia, H.; Ni, Q. Q. "Bridge" Graphene Oxide Modified Positive Charged Nanofiltration Thin Membrane with High Efficiency for Mg^{2+}/Li^+ Separation. *Desalination* **2020**, *488*. https://doi.org/10.1016/j.desal.2020.114522.

(33) Xu, P.; Hong, J.; Xu, Z.; Xia, H.; Ni, Q. Q. Positively Charged Nanofiltration Membrane Based on (MWCNTs-COOK)-Engineered Substrate for Fast and Efficient Lithium Extraction. *Sep Purif Technol* **2021**, *270*. https://doi.org/10.1016/j.seppur.2021.118796.

(34) Wang, L.; Rehman, D.; Sun, P. F.; Deshmukh, A.; Zhang, L.; Han, Q.; Yang, Z.; Wang, Z.; Park, H. D.; Lienhard, J. H.; Tang, C. Y. Novel Positively Charged Metal-Coordinated Nanofiltration Membrane for Lithium Recovery. *ACS Appl Mater Interfaces* **2021**, *13* (14), 16906–16915. https://doi.org/10.1021/acsami.1c02252.

(35) Yang, Y.; Li, Y.; Goh, K.; Tan, C. H.; Wang, R. Dopamine-Intercalated Polyelectrolyte Multilayered Nanofiltration Membranes: Toward High Permselectivity and Ion-Ion Selectivity. *J Memb Sci* **2022**, *648*. https://doi.org/10.1016/j.memsci.2022.120337.

(36) He, R.; Dong, C.; Xu, S.; Liu, C.; Zhao, S.; He, T. Unprecedented Mg^{2+}/Li^+ Separation Using Layer-by-Layer Based Nanofiltration Hollow Fiber Membranes. *Desalination* **2022**, *525*, 115492. https://doi.org/10.1016/J.DESAL.2021.115492.

(37) Braeken, L.; Bettens, B.; Boussu, K.; Van der Meeren, P.; Cocquyt, J.; Vermant, J.; Van der Bruggen, B. Transport Mechanisms of Dissolved Organic Compounds in Aqueous Solution during Nanofiltration. *J Memb Sci* **2006**, *279* (1–2), 311–319. https://doi.org/10.1016/J.MEMSCI.2005.12.024.

(38) Bruni, L.; Bandini, S. The Role of the Electrolyte on the Mechanism of Charge Formation in Polyamide Nanofiltration Membranes. *J Memb Sci* **2008**, *308* (1–2), 136–151. https://doi.org/10.1016/J.MEMSCI.2007.09.061.

(39) Yaroshchuk, A. E. Negative Rejection of Ions in Pressure-Driven Membrane Processes. *Adv Colloid Interface Sci* **2008**, *139* (1–2), 150–173. https://doi.org/10.1016/J.CIS.2008.01.004.

(40) Roy, Y.; Warsinger, D. M.; Lienhard, J. H. Effect of Temperature on Ion Transport in Nanofiltration Membranes: Diffusion, Convection and Electromigration. *Desalination* **2017**, *420*, 241–257. https://doi.org/10.1016/J.DESAL.2017.07.020.

(41) Lu, D.; Yao, Z.; Jiao, L.; Waheed, M.; Sun, Z.; Zhang, L. Separation Mechanism, Selectivity Enhancement Strategies and Advanced Materials for Mono-/Multivalent Ion-Selective Nanofiltration Membrane. *Advanced Membranes* **2022**, *2*, 100032. https://doi.org/10.1016/J.ADVMEM.2022.100032.

(42) Zhai, X.; Wang, Y. L.; Dai, R.; Li, X.; Wang, Z. Roles of Anion-Cation Coupling Transport and Dehydration-Induced Ion-Membrane Interaction in Precise Separation of Ions by Nanofiltration Membranes. *Environ Sci Technol* **2022**, *56* (19), 14069–14079. https://doi.org/10.1021/acs.est.2c04772.

(43) Merkel, A.; Voropaeva, D.; Ondrušek, M. The Impact of Integrated Nanofiltration and Electrodialytic Processes on the Chemical Composition of Sweet and Acid Whey Streams. *J Food Eng* **2021**, *298*, 110500. https://doi.org/10.1016/J.JFOODENG.2021.110500.

(44) Merdaw, A. A.; Sharif, A. O.; Derwish, G. A. W. Mass Transfer in Pressure-Driven Membrane Separation Processes, Part II. *Chemical Engineering Journal* **2011**, *168* (1), 229–240. https://doi.org/10.1016/J.CEJ.2010.12.072.

(45) Sigurdardottir, S. B.; DuChanois, R. M.; Epsztein, R.; Pinelo, M.; Elimelech, M. Energy Barriers to Anion Transport in Polyelectrolyte Multilayer Nanofiltration

Membranes: Role of Intra-Pore Diffusion. *J Memb Sci* **2020**, *603*, 117921. https://doi.org/10.1016/J.MEMSCI.2020.117921.

(46) Tansel, B. Significance of Thermodynamic and Physical Characteristics on Permeation of Ions during Membrane Separation: Hydrated Radius, Hydration Free Energy and Viscous Effects. *Sep Purif Technol* **2012**, *86*, 119–126. https://doi.org/10.1016/J.SEPPUR.2011.10.033.

(47) Yaroshchuk, A. E. *Non-Steric Mechanisms of Nanofiltration: Superposition of Donnan and Dielectric Exclusion*; **2001**; Vol. 22. www.elsevier.com/locate/seppur.

(48) Chen, B.; Jiang, H.; Liu, X.; Hu, X. Molecular Insight into Water Desalination across Multilayer Graphene Oxide Membranes. *ACS Appl Mater Interfaces* **2017**, *9* (27), 22826–22836. https://doi.org/10.1021/acsami.7b05307.

(49) Bowen, W. R.; Mohammad, A. W.; Hilal, N. Characterisation of Nanofiltration Membranes for Predictive Purposes — Use of Salts, Uncharged Solutes and Atomic Force Microscopy. *J Memb Sci* **1997**, *126* (1), 91–105. https://doi.org/10.1016/S0376-7388(96)00276-1.

(50) Szymczyk, A.; Fievet, P. Investigating Transport Properties of Nanofiltration Membranes by Means of a Steric, Electric and Dielectric Exclusion Model. *J Memb Sci* **2005**, *252* (1–2), 77–88.
https://doi.org/10.1016/J.MEMSCI.2004.12.002.

(51) Oatley, D. L.; Llenas, L.; Pérez, R.; Williams, P. M.; Martínez-Lladó, X.; Rovira, M. Review of the Dielectric Properties of Nanofiltration Membranes and Verification of the Single Oriented Layer Approximation. *Adv Colloid Interface Sci* **2012**, *173*, 1–11. https://doi.org/10.1016/J.CIS.2012.02.001.

(52) Gungormus, E.; Seker, E.; Alsoy Altinkaya, S. Antifouling Polydopamine-Modified Poly (Ether Sulfone) Membrane Immobilized With Alumina-Calcium Oxide Catalyst For Continuous Biodiesel Production. *Fuel* **2023**, *349*.
https://doi.org/10.1016/j.fuel.2023.128685.

(53) He, R.; Xu, S.; Wang, R.; Bai, B.; Lin, S.; He, T. Polyelectrolyte-Based Nanofiltration Membranes with Exceptional Performance in Mg^{2+}/Li^+ Separation in a Wide Range of Solution Conditions. *J Memb Sci* **2022**, *663*.
https://doi.org/10.1016/j.memsci.2022.121027.

(54) Li, H.; Wang, Y.; Li, T.; Ren, X. K.; Wang, J.; Wang, Z.; Zhao, S. Nanofiltration Membrane with Crown Ether as Exclusive Li^+ Transport Channels Achieving

Efficient Extraction of Lithium from Salt Lake Brine. *Chemical Engineering Journal* **2022**, *438*. https://doi.org/10.1016/j.cej.2022.135658.

(55) Rathi, P. B.; Mourya, V. K. *Extended Hildebrand Solubility Approach: Satranidazole in Mixtures of Dioxane and Water Rathi and Mourya: Solubility Prediction of Satranidazole in Dioxane-Water Mixtures*; **1997**; Vol. 14. www.ijpsonline.com.

(56) Pulyalina, A.; Rostovtseva, V.; Minich, I.; Silyukov, O.; Toikka, M.; Saprykina, N.; Polotskaya, G. Specific Structure and Properties of Composite Membranes Based on the Torlon® (Polyamide-Imide)/Layered Perovskite Oxide. *Symmetry (Basel)* **2020**, *12* (7). https://doi.org/10.3390/sym12071142.

(57) Hansen, C. M. *Hansen Solubility Parameters A User's Handbook Second Edition*; **2007**.

(58) Qiu, W.-Z.; Yang, H.-C.; Xu, Z.-K. Dopamine-Assisted Co-Deposition: An Emerging and Promising Strategy for Surface Modification. *Adv Colloid Interface Sci* **2018**, *256*, 111–125. https://doi.org/10.1016/j.cis.2018.04.011.

(59) Burzio, L. A.; Waite, J. H. Cross-Linking in Adhesive Quinoproteins: Studies with Model Decapeptides. *Biochemistry* **2000**, *39* (36), 11147–11153. https://doi.org/10.1021/bi0002434.

(60) Yu, B.; Liu, J.; Liu, S.; Zhou, F. Pdop Layer Exhibiting Zwitterionicity: A Simple Electrochemical Interface for Governing Ion Permeability. *Chemical Communications* **2010**, *46* (32), 5900. https://doi.org/10.1039/c0cc00596g.

(61) Kim, K.-Y.; Yang, E.; Lee, M.-Y.; Chae, K.-J.; Kim, C.-M.; Kim, I. S. Polydopamine Coating Effects on Ultrafiltration Membrane to Enhance Power Density and Mitigate Biofouling of Ultrafiltration Microbial Fuel Cells (UF-MFCs). *Water Res* **2014**, *54*, 62–68. https://doi.org/10.1016/j.watres.2014.01.045.

(62) Li, C.; Yang, Q.; Chen, D.; Zhu, H.; Chen, J.; Liu, R.; Dang, Q.; Wang, X. Polyethyleneimine-Assisted Co-Deposition of Polydopamine Coating with Enhanced Stability and Efficient Secondary Modification. *RSC Adv* **2022**, *12* (54), 34837–34849. https://doi.org/10.1039/D2RA05130C.

(63) Bi, Q.; Zhang, Z.; Zhao, C.; Tao, Z. Study on the Recovery of Lithium from High Mg^{2+}/Li^+ Ratio Brine by Nanofiltration. *Water Science and Technology* **2014**, *70* (10), 1690–1694. https://doi.org/10.2166/wst.2014.426.

(64)   Sata, T. Studies on Anion Exchange Membranes Having Permselectivity for Specific Anions in Electrodialysis — Effect of Hydrophilicity of Anion Exchange Membranes on Permselectivity of Anions. *J Memb Sci* **2000**, *167* (1), 1–31. https://doi.org/10.1016/S0376-7388(99)00277-X.

(65)   Li, W.; Shi, C.; Zhou, A.; He, X.; Sun, Y.; Zhang, J. A Positively Charged Composite Nanofiltration Membrane Modified by EDTA for $LiCl/MgCl_2$ Separation. *Sep Purif Technol* **2017**, *186*, 233–242. https://doi.org/10.1016/j.seppur.2017.05.044.

(66)   Wu, H.; Lin, Y.; Feng, W.; Liu, T.; Wang, L.; Yao, H.; Wang, X. A Novel Nanofiltration Membrane with [MimAP][Tf2N] Ionic Liquid for Utilization of Lithium from Brines with High Mg^{2+}/Li^+ Ratio. *J Memb Sci* **2020**, *603*. https://doi.org/10.1016/j.memsci.2020.117997.

(67)   Chen, K.; Zhao, S.; Lan, H.; Xie, T.; Wang, H.; Chen, Y.; Li, P.; Sun, H.; Niu, Q. J.; Yang, C. Dual-Electric Layer Nanofiltration Membranes Based on Polyphenol/PEI Interlayer for Highly Efficient Mg^{2+}/Li^+ Separation. *J Memb Sci* **2022**, *660*. https://doi.org/10.1016/j.memsci.2022.120860.